Electrokinetics of a particle attached to a fluid interface: Electrophoretic mobility and interfacial deformation

Michael Eigenbrod, Florian Bihler, and Steffen Hardt[*]

Institute for Nano- and Microfluidics, Technische Universität Darmstadt, 64287 Darmstadt, Germany

The electrophoretic mobility of a microparticle with a small ζ potential attached to a fluid interface is studied analytically in the limit of two fluids with vanishing viscosity and permittivity ratios under the assumption of a weak applied electric field. The analysis is based on perturbation expansions in the capillary number, the electric capillary number, and in the deviation of the contact angle on the particle surface from $90°$. For the case of a very thin electric double layer (EDL), the Smoluchowski limit for the electrophoretic mobility is recovered. For arbitrary values of the EDL thickness, a spherical particle is considered. In that case the electrophoretic mobility is a function of the EDL thickness and the contact angle at the particle surface. Hydrophobic particles have a higher mobility than hydrophilic ones. The deformation of the fluid interface is shown to be separable into a dynamic and static part. The motion of the particle (dynamic part) does not contribute to the interfacial deformation in the case of a small capillary number, even for arbitrary EDL thickness. The static interfacial deformation due to electric stresses, known as electrodipping, is examined for spherical particles and shown to be independent of the first-order perturbation in the contact angle. The limits of validity of our theory and possible applications are discussed.

I. INTRODUCTION

Electrophoresis is probably one of the most important electrokinetic phenomena, with applications in analytical chemistry [see, e.g., Refs. 1–3], among others, where it is mostly used for the separation of molecules or particles. Moreover, it is one of the most prominent principles lab-on-a-chip devices are based on [see, e.g., Refs. 4–6].

Whenever a charged particle, surrounded by an electrolyte, is subjected to an external electric field, it starts to move into the direction of the oppositely charged electrode. If the constant applied electric field is not too strong, the velocity of the particle U takes the form [7,8]

$$U = \eta E_\infty, \tag{1}$$

in which η is the electrophoretic mobility and E_∞ the magnitude of the applied electric field. The electrophoretic mobility depends on the thickness of the electric double layer (EDL) (called Debye length κ^{-1}) around the particle, which develops as a consequence of the charge of the particle. Pioneering work addressing the electrophoretic mobility of spherical particles was carried out by von Smoluchowski [9], Hückel [10], and Henry [11]. Von Smoluchowski [9] studied the electrophoretic mobility of spherical particles in the limit of thin EDLs (thin Debye length, $\kappa \to \infty$) and found the well-known Smoluchowski limit $\eta = \frac{\epsilon\zeta}{\mu}$, where ϵ, μ, ζ are the permittivity and the

---

*[*]hardt@nmf.tu-darmstadt.de

viscosity of the electrolyte and the ζ potential of the particle, respectively. The small Debye length assumption holds for many particles, since the EDL thickness is often much smaller than the size of the particle [12]. As an extension of Smoluchowski's work, Morrison [13] and Teubner [14] proved that the Smoluchowski limit holds for particles of arbitrary shape. For the case that the size of the particle is very small compared to the Debye layer thickness, Hückel [10] found a reduction of the electrophoretic mobility, i.e., $\eta = \frac{2}{3}\frac{\epsilon\zeta}{\mu}$. Under certain assumptions (e.g., rotationally symmetric EDLs), Henry [11] generalized the theory for spherical (and cylindrical) particles and confirmed the Smoluchowski and Hückel theories as limiting cases. An extension of Henry's work was done by Overbeek [7] and Booth [15]. Both authors studied the deformation of the EDL, called relaxation effect, occurring for highly charged particles. A high charge corresponds to a significant flow leading to a deformation of the EDL. They found that for moderate values of the Debye length, i.e., $0.2 < \kappa a < 50$ (a is the radius of the spherical particle), the relaxation effect leads to corrections of the electrophoretic mobility. Wiersema *et al.* [16] provided extensions of the previous studies in the form of numerical simulations and discussed the limits of validity of foregoing work. Later on, boundary effects [17–20] and the interaction of two particles in the thin [21] and thick Debye layer limit [22] have been studied.

In many practical applications, particles are not suspended in the bulk of a fluid, but are attached to a fluid interface. Examples are drops covered with particles (so-called liquid marbles) [23] and pickering emulsions [24]. The study of electrophoretic phenomena at fluid interfaces is still at its infancy, due to the complex interplay between hydrodynamics, electrostatics, and the deformation of the interface separating the two fluids. In that context, a number of fundamental questions related to the structure of fluid interfaces are still open. For example, the charge of a fluid interface is still a matter of controversial discussion. There are experimental indications that the water-air interface carries a negative charge [see, e.g., Refs. 25–27]. Other experimental papers report a positive charge [see, e.g., Refs. 28–30]. Theoretical/numerical results also vary in magnitude and sign, predict either a positive [see, e.g., Refs. 31,32] or a negative [see, e.g., Refs. 33,34] charge at the water-air interface. These inconsistencies may be partially due to the difficulty of a direct measurement [see Ref. 35] and due to differences in the modeling approaches [see Ref. 36].

In theoretical studies of electrophoresis close to fluid interfaces, usually an uncharged interface is assumed. Tsai *et al.* [37] studied the electrophoretic motion of a spherical particle normal to an uncharged, undeformable and flat air-water interface for different Debye layer thicknesses. The motion parallel to a flat liquid-fluid interface was studied by Gao and Li [38] in the thin Debye layer limit. Apart from the dynamic particle-interface interaction, researchers found a static interface deformation caused by the charge of the particle attached to the interface between an aqueous phase and an unpolar fluid. This effect was termed "electrodipping." Due to the difference in the dielectric constants of both fluids and an inhomogeneous surface charge of the particle, a force arises that pulls the particle into the fluid with the higher permittivity [39]. In their experiments, Nikolaides *et al.* [39] and Aveyard *et al.* [40] found a long-range interaction between interfacial particles which gave rise to controversial discussions [41–47]. Danov *et al.* [43,45] performed experiments for glass particles at water-oil and water-air interfaces and found an interaction of interfacial particles with a shorter range than Nikolaides *et al.* [39]. Moreover, they found that the electrodipping force in a water-oil system is much higher than in a water-air system. In all theoretical works, the authors claim that the force inside the nonpolar fluid acting on the particle is much higher than the force inside the electrolyte [39,42–47]. However, all corresponding theoretical studies are limited to thin Debye layers. Independently from each other, several authors reported an interfacial deformation decaying like $h \propto r^{-4}$, in which h and r denote the height of the fluid interface and the distance from the particle, respectively [41–47].

In the following, we analyze the electrophoretic transport of a particle attached to a fluid interface. The limiting case of large contrasts between the viscosities and the dielectric permittivities of the two fluids is considered. In Sec. II we describe the problem and the model assumptions. Subsequently, we specify the governing equations together with the corresponding boundary
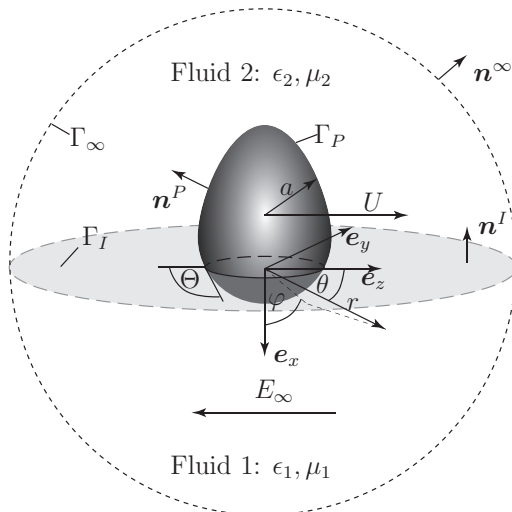
FIG. 1. Schematic of a particle attached to a fluid interface. Without loss of generality, we assume the negatively charged particle to move with a velocity U in the positive z direction due to an constant applied electric field E_∞. The contact angle of the fluid interface at the particle surface is denoted by Θ, and a stands for a characteristic length scale. Γ_P, Γ_I, and Γ_∞, denote the particle, the fluid interface and the far field domain, i.e., a sphere with a radius of $r \to \infty$, respectively. The normal vectors corresponding to the three boundaries of the fluid domain are denoted by n^I, n^P, and n^∞. The origin of the coordinate system lies in the plane of the undeformed fluid interface.

conditions. In Sec. III, we derive general relationships valid for particles of a broad class of geometrical shapes. In Sec. IV, the case of a spherical particle is discussed. Apart from the electrophoretic mobility, we also study the interfacial deformation. Further, in Sec. V, we discuss the limits of validity of our theory and a possible application in terms of electrophoretic separation. Finally, in Sec. VI we summarize the main results of our work and give an outlook to further studies.

II. PROBLEM FORMULATION AND MODEL ASSUMPTIONS

We consider the motion of a particle, whose size is characterized by a length scale a, attached to a fluid interface in an unbounded domain in the presence of an uniform applied electric field; see Fig. 1. In this study we focus on the translational electrophoretic motion of neutrally buoyant particles at small Reynolds numbers Re $\ll$ 1. Both fluid phases are considered to be incompressible Newtonian fluids with constant viscosities μ_i and dielectric permittivities ϵ_i, with $i = 1, 2$ denoting the two different phases. The particle attached to the fluid interface is assumed to be in a stationary-state configuration.

The foregoing assumptions still leave us with a very general problem and do not simplify the governing equation sufficiently to enable an analytical treatment. Therefore, the following assumptions are added, to be further explained in subsequent sections:

(1) The applied electric field E_∞ is uniform and weak;

(2) The ζ potential at the particle surface is small and uniform over each surface portion in contact with a specific fluid;

(3) The fluid interface is chargeless $q_{sf} = 0$;

(4) The viscosity and permittivity ratios asymptotically vanish, i.e., $\frac{\mu_2}{\mu_1} \to 0$ and $\frac{\epsilon_2}{\epsilon_1} \to 0$.

In linear electrophoresis, the electrophoretic mobility is defined as the constant of proportionality between the velocity of the particle U and the applied electric field E_∞ [see Eq. (1)]. The splitting of the electrostatic potential into a sum of an equilibrium potential, corresponding to the Debye layer

around the particle, and a perturbation potential due to the applied electric field is a consequence of assumption 1 if the relaxation of the EDL is neglected. Together with assumption 2, this leads to a Boltzmann distribution of the ion number density around the particle [see Ref. 48]. Consequently, the Debye layer around the particle has a uniform thickness in each of the two fluids, apart from small deviations close to the three-phase contact line [49]. Whether or not a Debye layer also forms at the fluid interfaces depends, among others, on the presence of ionic surfactants. We assume a surfactant-free interface. Moreover, we do not enter the controversial discussion about the charge of the fluid interface and assume, for simplicity, that one of the following two statements is valid:

(1) The ζ potential of the fluid interface is small compared to the one of the particle.
(2) The Debye length is much smaller than a.

Referring to the second statement, even in the case of a charged interface, a thin Debye layer compared to the characteristic size of the particle ensures that the fluid interface can be regarded as overall electroneutral on the particle scale. Note that in this work we do not generally assume a thin Debye layer, but also consider thick Debye layers. The assumption of an asymptotically vanishing viscosity and permittivity ratio is fulfilled reasonably well if the two fluids are water and air: $\frac{\mu_2}{\mu_1} \approx 0.02$ [see, e.g., Ref. 50] and $\frac{\epsilon_2}{\epsilon_1} \approx 0.01$ [see, e.g., Ref. 51] at typical laboratory conditions. The assumptions 1 and 2 were also employed in the classical paper of Henry [11] as well as in more recent articles addressing the electrophoretic mobility corresponding to different particle geometries [52,53]. Although recent articles dealing with the electrophoresis of particles in a bulk electrolyte rely on less restrictions and assumptions concerning, e.g., the strength of the applied electric field [see, e.g., Ref. 54], it is reasonable to start solving a significantly more complicated problem along the lines of the classical theory of electrophoresis to keep the calculations manageable.

A. Governing equations and boundary conditions

The set of governing equations, consisting of the quasistatic Stokes equations with an additional volume force, the continuity equation, the Poisson equation, and the Nernst-Planck equations, coupling the ion concentrations with the electric field and the flow field of the medium, have been derived by Overbeek [7]. We formally consider a small perturbation from equilibrium due to the applied electric field, which is a common assumption [e.g., Refs. 8,16]. When the ion concentration fields are assumed to be unaffected by the external field, i.e., the relaxation effect of the EDL is neglected, the set of the governing equations can be written as

$$-\nabla p_i^{\mathrm{d}} + \mu_i \nabla^2 \boldsymbol{v}_i + \epsilon_i \nabla^2 \psi_i \nabla \phi_i = \boldsymbol{0}, \tag{2}$$

$$-\nabla p_i^{\mathrm{s}} + \epsilon_i \nabla^2 \psi_i \nabla \psi_i = \boldsymbol{0}, \tag{3}$$

$$\nabla \cdot \boldsymbol{v}_i = 0, \tag{4}$$

$$\nabla^2 \psi_i = \kappa_i^2 \psi_i, \tag{5}$$

$$\nabla^2 \phi_i = 0, \tag{6}$$

in which p_i^{d} is the dynamic pressure, p_i^{s} is the static pressure corresponding to the equilibrium state, $\boldsymbol{v}_i$ is the velocity and κ_i is the inverse Debye length. The subscripts denote the phases $i = 1, 2$. Equations (2) and (4) are the Stokes and continuity equations, while Eqs. (5) and (6) are the linearized Poisson-Boltzmann and Laplace equation, respectively. Equation (3) is the momentum equation corresponding to the equilibrium system without an applied electric field. The term $\epsilon_i \nabla^2 \psi_i \nabla \psi_i$ is proportional to the square of the ζ potential of the particle, which clearly does not contribute to the electrophoretic mobility [see Refs. 11,14,52,53]. For interfacial particles, as we will show later, Eq. (3) is responsible for the deformation of the fluid interface.

Before we continue to formulate appropriate boundary conditions, we rewrite Eqs. (2)–(6) in dimensionless form, by defining

$$\nabla = \frac{\bar{\nabla}}{a}, \quad \boldsymbol{v}_i = U\bar{\boldsymbol{v}}_i, \quad p_i^{\mathrm{d}} = \frac{\mu_1 U}{a}\bar{p}_i^{\mathrm{d}}, \quad p_i^{\mathrm{s}} = \frac{\epsilon_1 \zeta_1^2}{a^2}\bar{p}_i^{\mathrm{s}}, \quad \psi_i = \zeta_1\bar{\psi}_i, \quad \phi_i = E_\infty a\bar{\phi}_i, \quad \eta = \frac{\epsilon_1 \zeta_1}{\mu_1}\bar{\eta},$$
(7)

and arrive at

$$-\bar{\nabla}\bar{p}_1^{\mathrm{d}} + \bar{\nabla}^2\bar{\boldsymbol{v}}_1 + \frac{1}{\bar{\eta}}\bar{\nabla}^2\bar{\psi}_1\bar{\nabla}\bar{\phi}_1 = \boldsymbol{0},$$
(8)

$$-\bar{\nabla}\bar{p}_2^{\mathrm{d}} + \frac{\mu_2}{\mu_1}\bar{\nabla}^2\bar{\boldsymbol{v}}_2 + \frac{\epsilon_2}{\epsilon_1}\frac{1}{\bar{\eta}}\bar{\nabla}^2\bar{\psi}_2\bar{\nabla}\bar{\phi}_2 = \boldsymbol{0},$$
(9)

$$-\bar{\nabla}\bar{p}_1^{\mathrm{s}} + \bar{\nabla}^2\bar{\psi}_1\bar{\nabla}\bar{\psi}_1 = \boldsymbol{0},$$
(10)

$$-\bar{\nabla}\bar{p}_2^{\mathrm{s}} + \frac{\epsilon_2}{\epsilon_1}\bar{\nabla}^2\bar{\psi}_2\bar{\nabla}\bar{\psi}_2 = \boldsymbol{0},$$
(11)

$$\bar{\nabla} \cdot \bar{\boldsymbol{v}}_i = 0,$$
(12)

$$\bar{\nabla}^2\bar{\psi}_i - (\kappa_i a)^2\bar{\psi}_i = 0,$$
(13)

$$\bar{\nabla}^2\bar{\phi}_i = 0.$$
(14)

In general, the fluid domain is modeled to be bounded by three surfaces, i.e., the particle surface Γ_P, the fluid interface Γ_I and the bounding sphere Γ_∞ corresponding to $r \rightarrow \infty$, as shown in Fig. 1. First, we focus on Γ_P and Γ_∞ and formulate the following conditions [see Refs. 11,14,53] in dimensionless form:

$$\bar{p}_i^{\mathrm{s}}\big|_{\Gamma_\infty} \rightarrow 0, \quad \bar{p}_i^{\mathrm{d}}\big|_{\Gamma_\infty} \rightarrow 0, \quad \bar{\boldsymbol{v}}_i\big|_{\Gamma_\infty} \rightarrow \boldsymbol{0}, \quad \bar{\psi}_i\big|_{\Gamma_\infty} \rightarrow 0, \quad \bar{\phi}_i\big|_{\Gamma_\infty} = \bar{r}\cos(\theta),$$
(15)

$$\bar{\boldsymbol{v}}_i\big|_{\Gamma_P} = \boldsymbol{e}_z, \quad \bar{\psi}_1\big|_{\Gamma_P} = 1, \quad \bar{\psi}_2\big|_{\Gamma_P} = \frac{\zeta_2}{\zeta_1}, \quad \frac{\partial\bar{\phi}_i}{\partial\boldsymbol{n}}\bigg|_{\Gamma_P} = 0.$$
(16)

Without loss of generality, we assume the particle to be negatively charged with a corresponding motion in $\boldsymbol{e}_z$-direction. The zero gradient condition for the perturbation potential $\bar{\phi}$ at the surface of the particle results from an additional condition, i.e., the permittivity of the particle ϵ_P is small in comparison to the permittivity of its surrounding media, which at first glance appears to be a very limiting assumption. However, as shown by O'Brien and White [8], the electrophoretic mobility is independent of the boundary condition at the particle surface, and therefore the assumption $\epsilon_P \ll \epsilon_i$ does not necessarily need to be satisfied. When applying assumption 4 to Eqs. (9) and (11) and considering the boundary conditions [see Eq. (15)] one finds a vanishing dynamic and static pressure in phase 2. Therefore, on the basis of our assumptions, it is not necessary to consider phase 2 in our theoretical analysis. Hence, we omit the index labeling of the phases from now on, with the convention that all quantities refer to phase 1. However, it is worth mentioning that $\epsilon_P \ll \epsilon_1$ is usually valid if phase 1 is an aqueous solution.

The boundary conditions at the fluid interface can be obtained by integrating the governing equations across the interface [see Refs. 55–59]. The empirical no-slip condition [see Ref. 58], together with the integration of Eq. (4), leads to a continuous velocity field across the fluid interface and can be written in jump-bracket notation $[[\Sigma]] := \lim_{\epsilon \rightarrow 0}(\Sigma_2(\boldsymbol{r} + \epsilon\boldsymbol{n}) - \Sigma_1(\boldsymbol{r} - \epsilon\boldsymbol{n}))$ as [see Refs. 55,56,59]

$$[[\bar{\boldsymbol{v}}]] = \boldsymbol{0}.$$
(17)

The boundary conditions for the electrostatic problem can be obtained by integrating the Poisson equation. Following Jackson [56] and inserting the decomposition of the electrostatic potential, we

find (see assumption 3)

$$\boldsymbol{n} \cdot [\![\epsilon \nabla(\psi + \phi)]\!] = 0. \tag{18}$$

$\psi + \phi$ is the sum of an equilibrium potential and a slight disturbance due to the applied electric field [11]. Therefore, it is reasonable to assume that Eq. (18) must hold separately for both potentials. Taking assumptions 3 and 4 into account, we find

$$\frac{\partial \bar{\psi}_1}{\partial \boldsymbol{n}} = 0, \tag{19}$$

$$\frac{\partial \bar{\phi}_1}{\partial \boldsymbol{n}} = 0. \tag{20}$$

B. Deformation of the fluid interface

On the basis of Eqs. (2) and (3), there are two possible ways for a neutrally buoyant and charged particle to deform the fluid interface it is attached to. On one hand, one might think of a deformation due to the motion of the particle, e.g., a translation of the particle with the particle axis at a tilted angle [see 60]. On the other hand, a static deformation caused by the electric field, which is known as electrodipping [see Refs. 39,42–44], might occur. Because of the linearity of the governing equations, the static and dynamic effects can be separated into two independent equations. By defining

$$\bar{\mathbf{T}} = \bar{\nabla}\bar{\boldsymbol{v}} + (\bar{\nabla}\bar{\boldsymbol{v}})^T, \tag{21}$$

$$\bar{\mathbf{M}}^{\mathrm{s}} = \bar{\nabla}\bar{\psi} \otimes \bar{\nabla}\bar{\psi} - \tfrac{1}{2}\bar{\nabla}\bar{\psi} \cdot \bar{\nabla}\bar{\psi}\boldsymbol{I}, \tag{22}$$

$$\bar{\mathbf{M}}^{\mathrm{d}} = \bar{\nabla}\bar{\psi} \otimes \bar{\nabla}\bar{\phi} + \bar{\nabla}\bar{\phi} \otimes \bar{\nabla}\bar{\psi} - \bar{\nabla}\bar{\psi} \cdot \bar{\nabla}\bar{\phi}\boldsymbol{I}, \tag{23}$$

and integration of the sum of Eqs. (2) and (3) across the interface, taking the interfacial tension force into account, we find [see Refs. 57–59]

$$\mathrm{Ca}\left(-\boldsymbol{n}\bar{p}^{\mathrm{d}} + \bar{\mathbf{T}} \cdot \boldsymbol{n} + \frac{1}{\bar{\eta}}\bar{\mathbf{M}}^{\mathrm{d}} \cdot \boldsymbol{n}\right) + \mathrm{Ce}(-\boldsymbol{n}\bar{p}^{\mathrm{s}} + \bar{\mathbf{M}}^{\mathrm{s}} \cdot \boldsymbol{n}) = \boldsymbol{n}(\bar{\nabla} \cdot \boldsymbol{n}), \quad \text{with} \tag{24}$$

$$\mathrm{Ca} = \frac{\mu_1 U}{\gamma} \quad \text{and} \quad \mathrm{Ce} = \frac{\epsilon_1 \zeta_1^2}{a\gamma}. \tag{25}$$

$\boldsymbol{n}$ is the normal vector at the interface, pointing from fluid 1 into fluid 2. Ca represents the relative strength of the viscous forces compared to the capillary forces and is denoted capillary number. Ce is the relative strength of the electrostatic forces compared to the capillary forces and is denoted electric capillary number. For a static particle attachment (no external applied electric field), the capillary number Ca becomes zero, in contrast to Ce. In the case of an electrophoretic motion of the particle, both terms contribute and lead to a combined interfacial deformation. Therefore electrodipping is covered by Eq. (24).

In the following, we expand all physical quantities of Eq. (24) in a perturbation series in Ca and Ce up to the linear order. The interfacial deformation is therefore a sum of an equilibrium contribution (zeroth order), depending on the shape of the contact line at the particle, and two first-order contributions due to the electrostatic and hydrodynamic forces acting on it, proportional to Ce and Ca, respectively. We define the term "equilibrium interface" as the interface corresponding to an uncharged but geometrically equivalent and stationary interfacial particle. It is worth mentioning that the contributions to the interfacial deformation proportional to Ce and Ca are solely determined by physical quantities corresponding to the equilibrium interface. In theoretical papers dealing with particle-interface interaction, the deformation is typically computed on the basis of solutions corresponding to an undeformed interface [see, e.g., Refs. 42,45], and is therefore a
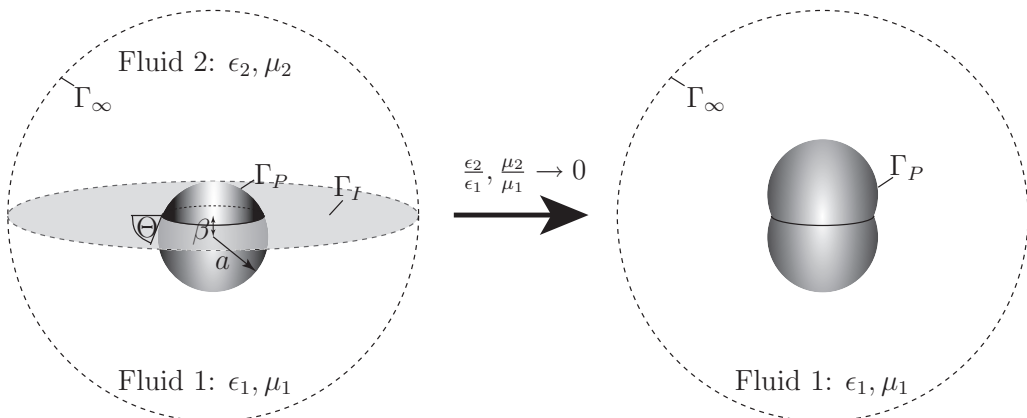
FIG. 2. Schematic of the two equivalent systems considered when computing the electrophoretic mobility of a sphere attached to a flat fluid interface. The electrophoretic mobility of a sphere attached to a flat fluid interface is equal to a the mobility of two spherical caps fused at the three-phase contact line. The perturbation parameter β represents the shift of the center of the sphere along the x direction relative to the fluid interface. a denotes the radius of the sphere.

first-order solution in the corresponding dimensionless number. We follow the same train of thought hereinafter.

III. ELECTROPHORESIS OF AN ARBITRARILY SHAPED PARTICLE

We consider an arbitrarily shaped particle characterized by a length scale a, attached to a fluid interface and translating with a velocity U due to an uniform applied electric field E_∞; see Fig. 1. Again, without loss of generality, we assume a negatively charged particle with a translational motion in $\boldsymbol{e}_z$-direction. To begin with, we consider particles with a three-phase contact line coplanar with the y, z plane. In this case, the equilibrium interface corresponds to a flat interface.

A. Electrophoretic mobility for a flat interface in the thin Debye layer limit, $\kappa a \to \infty$

In this paragraph we concentrate on the electrophoretic mobility of a particle attached to a flat interface. Usually, the electrophoretic mobility is obtained through a force balance at the particle [see Ref. 8], accounting for electrostatic and hydrodynamic forces. In contrast to this, we follow a different route by utilizing symmetry arguments as follows.

As already mentioned, fluid 2 does not contribute to the interfacial deformation or the electrophoretic mobility of the immersed particle; see Eqs. (9) and (11) and assumption 4. Furthermore, based on the boundary conditions, the flat fluid interface represents a symmetry boundary, leading to an equivalent problem formulation in which the part of the particle immersed in fluid 1 is mirror reflected at the flat interface (see Fig. 2). This results in two fused particle components in an unbounded electrolyte. In previous work [13,14] it was shown that the Smoluchowski [see Ref. 9] limit for the electrophoretic mobility holds no matter what the geometrical shape of the particle is. Therefore, such a particle has a electrophoretic mobility of

$$\bar{\eta} = 1, \quad \text{for } \kappa a \to \infty. \tag{26}$$

Equation (26) is a generalization of the Smoluchowski limit for particles attached to flat interfaces. Specifically, in the case of spherical particles Eq. (26) holds independent of the contact angle at the particle surface, determining its degree of immersion in fluid 1.

B. Effect of the dynamic interfacial deformation, $O(\text{Ca})$ and arbitrary κa

In this paragraph we focus on the interfacial deformation caused by the particle's motion up to linear order in Ca, but for arbitrary Debye length. When the corresponding momentum balance is integrated over the volume of fluid 1 and the divergence theorem is applied, a sum of three surface integrals, i.e., Γ_∞, Γ_I, and Γ_P, is obtained, representing the overall force balance. The forces acting on the boundary sufficiently far away from the particle vanish, which directly follows from the boundary conditions for $\bar{p}^d$, $\bar{\mathbf{v}}$, $\bar{\psi}$, and $\bar{\phi}$; see Eq. (15). As already mentioned, the electrophoretic mobility $\bar{\eta}$ is evaluated by a force balance at the particle. The net dimensionless forces acting on the particle must vanish, leading to a vanishing force at the fluid interface:

$$\int_{\Gamma_I} \left(\bar{\boldsymbol{\sigma}} \cdot \boldsymbol{n}_I + \frac{1}{\bar{\eta}} \bar{\mathbf{M}}^d \cdot \boldsymbol{n}_I \right) dS = \mathbf{0}. \tag{27}$$

If we assume a mirror-symmetric particle shape (see Fig. 1) with respect to the plane perpendicular to the direction of motion, i.e., the x, y plane (this holds for a large class of geometric shapes, i.e., spheres, spheroids, …), it is reasonable to assume that the integrand in Eq. (27) is odd with respect to z. For example, Dörr and Hardt [60] found an interfacial deformation described by an odd function, caused by fixed tilt angle of a spherical particle attached to a fluid interface and driven by an external force. The tilted position of the particle is caused by a hydrodynamic torque acting on it. Thus, it is useful to take the overall torque balance into account. The torque in the far field vanishes, therefore the torque acting on the particle ($\mathfrak{T}_P$) is equal to the torque acting on the fluid interface (since $\boldsymbol{n}_P = -\boldsymbol{n}^P$). For the evaluation of the interfacial deformation proportional to Ca we need to consider the torque acting on a flat interface, which can be written as

$$\mathfrak{T}_P = \int_0^{2\pi} \int_{\bar{r}_P(\theta)}^\infty \bar{r}^2 \boldsymbol{e}_r \times \left(\bar{\boldsymbol{\sigma}} \cdot \boldsymbol{n}_I + \frac{1}{\bar{\eta}} \bar{\mathbf{M}}^d \cdot \boldsymbol{n}_I \right) \Bigg|_{\varphi = \frac{\pi}{2}, \frac{3\pi}{2}} d\bar{r} \, d\theta, \quad \text{with} \quad \boldsymbol{n}_I = \pm \boldsymbol{e}_\phi. \tag{28}$$

In Appendix A, we show that for even parametrizations of the particle shape [i.e., $\bar{r}_P(-\theta) = \bar{r}_P(\theta)$] and odd integral kernels, Eq. (28) is identically zero. For this reason, there is no net torque acting on the particle, and consequently no tilting occurs. In other words, the sum of the hydrodynamic and electrostatic torque acting on the particle is identically zero. Therefore, to first order in Ca, the electrophoretic motion of the particle itself does not affect the interfacial deformation, leading to a pure electrostatic interfacial deformation proportional to Ce. However, the static interfacial deformation (proportional to Ce) cannot be quantified without any further specification of the particle shape. Hence, in the following we will concentrate on spherical particles attached to fluid interfaces, which is the case of highest practical relevance.

IV. ELECTROPHORETIC MOBILITY OF A SPHERICAL PARTICLE FOR ARBITRARY DEBYE LENGTH AND CORRESPONDING INTERFACIAL DEFORMATION

We consider a spherical particle attached to a fluid interface with a prescribed contact angle. A sphere clearly fulfills all symmetry constraints described in Secs. III A and III B. Hence, the electrophoretic mobility in the thin Debye layer limit is given by Eq. (26) and consequently independent of the contact angle or the size of the particle (as long as the underlying assumptions are satisfied). Moreover, the motion of the particle does not result in a deformation of the fluid interface up to first order in Ca. Therefore, the remaining task is the determination of the electrophoretic mobility for an arbitrary Debye length along with the electrostatic interfacial deformation. To lowest order, the interface is flat, so the configuration is equivalent to a system of fused spheres in an unbounded domain; see Fig. 2.

A. Electrophoretic mobility for a flat interface

We restrict our analysis to contact angles around $90°$. Based on that, by defining $\beta := \cos(\Theta)$, it follows that $\beta \ll 1$. This motivates us to let β take the role of a perturbation parameter [see Ref. 60].

In dimensionless form, β is directly linked to the vertical shift of the particle center relative to the flat interface; see Fig. 2. The parametrization of the fused spherical caps is given by

$$\bar{r} = \beta \sin(\theta)|\cos(\varphi)| + \sqrt{1 - \beta^2[1 - \sin^2(\theta)\cos^2(\varphi)]}, \tag{29}$$

or, expanded in terms of β:

$$\bar{r} \approx 1 + \beta f(\theta, \varphi) + O(\beta^2), \quad \text{with} \quad f(\theta, \varphi) = \sin(\theta)|\cos(\varphi)|. \tag{30}$$

We omit all terms of higher than linear order in β. The previous equation is a parametrization of a slightly deformed sphere. This type of geometry has been studied in Stokes flow without source terms [see Ref. 61], and in context with electrophoretic [see Ref. 53], thermophoretic [see Ref. 62] as well as diffusiophoretic motion [see Ref. 63]. Brenner [61], Kim and Yoon [53], Senchenko and Keh [62], and Khair [63] mapped the boundary conditions at the surface of a slightly deformed sphere to more complex boundary conditions (depending on θ and φ) for an undeformed sphere. Every function defined on a sphere can be expanded into an infinite sum of spherical harmonics [see, e.g., Refs. 56,64,65]. After expanding the mapped boundary conditions into an infinite sum of spherical harmonics, the remaining task is to find (an infinite number of) functions that satisfy the governing equations together with the expanded boundary conditions at the surface of the sphere and the far-field boundary condition. Kim and Yoon [53] used an equivalent method, i.e., a multipole expansion of the boundary conditions up to the quadrupole moment that corresponds to a sum representation up to the second partial sum, which is sufficient, since higher partial sums do not contribute to the electrophoretic mobility. By contrast to the approach employed by Kim and Yoon [53], we follow Byerly [64]'s sum representation that avoids a large number of matrix manipulations and gives a better insight into the structure of the solution. An advantage of the domain perturbation method is its stepwise structure. The zeroth-order solution (in β) specifies the boundary conditions for the first-order perturbation analysis, as we show in Appendix B. We expand all physical quantities in the new perturbation parameter β, e.g.,

$$\bar{p}^d = \bar{p}^d_{(0)} + \beta \, \bar{p}^d_{(1)} + O(\beta^2), \tag{31}$$

and we again omit all terms beyond linear order.

In Appendix B we derive the solutions of the governing equations to zeroth and first order in β. The zeroth-order approximation corresponds to the famous solution first obtained by Henry [see Ref. 11]:

$$\bar{\eta}_{(0)} = \tfrac{1}{144}[96 + (\kappa a)^2(3 + \kappa a)(2 + (\kappa a - 4)\kappa a) + e^{\kappa a}(\kappa a)^4((\kappa a)^2 - 12)\text{Ei}(-\kappa a)]. \tag{32}$$

$\text{Ei}(x)$ is the exponential integral function, defined by

$$\text{Ei}(x) = -\int_{-x}^{\infty} \frac{\exp(-t)}{t} dt. \tag{33}$$

As expected, the Smoluchowski [9] ($\kappa a \to \infty$) and the Hückel [10] ($\kappa a \to 0$) limits can formally be obtained from Eq. (32). In the context considered here, the expression holds for a spherical particle attached to a flat interface with a contact angle of $\Theta = 90°$.
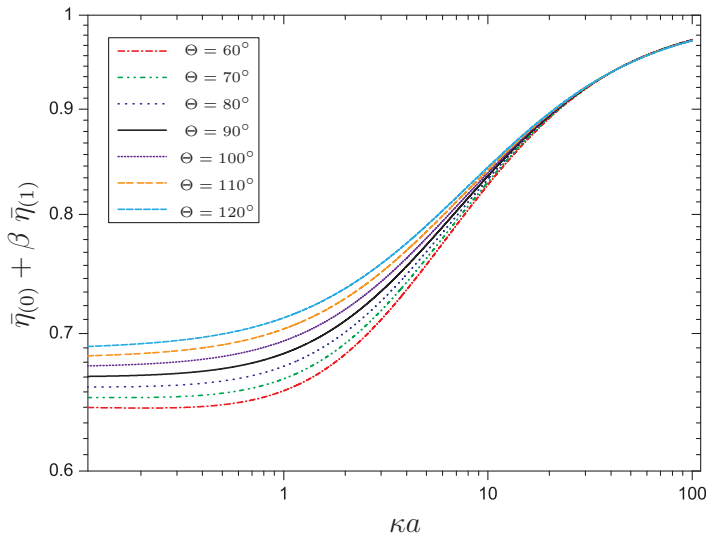
FIG. 3. Electrophoretic mobility of a spherical particle attached to a flat fluid interface as a function of the Debye parameter for different contact angles $\beta = \cos(\Theta)$.

Following Appendix B 2, we obtain the first-order (in β) correction to the electrophoretic mobility

$$
\begin{aligned}
\bar{\eta}_{(1)} = {} & \frac{1}{1536(3 + \kappa a(3 + \kappa a))}[-192 + \kappa a\{-384 + \kappa a(24 + \kappa a\{-304 \\
& + \kappa a(-726 + \kappa a\{-352 + \kappa a(27 + \kappa a\{46 + 5\kappa a\})\})\})\} \\
& + \exp(\kappa a)(\kappa a)^4(-840 + \kappa a\{-1032 + \kappa a(-356 + \kappa a\{68 + \kappa a(51 + 5\kappa a)\})\}) \mathsf{Ei}(-\kappa a)].
\end{aligned}
$$
(34)

Figure 3 shows the electrophoretic mobility of a spherical particle attached to a flat fluid interface as a function of the contact angle and the Debye parameter. As expected, the Smoluchowski limit remains unaffected by the value of the contact angle; see Eq. (26). More specifically, the electrophoretic mobility is nearly independent of the contact angle if the Debye parameter κa is above 30. The electrophoretic mobility in the Hückel limit ($\kappa a \to 0$) is readily obtained as

$$
\lim_{\kappa a \to 0}(\bar{\eta}_{(0)} + \beta\,\bar{\eta}_{(1)}) = \frac{2}{3} - \frac{\beta}{24}.
$$
(35)

In this limit the electrophoretic mobility increases with increasing contact angle. Therefore, with increasing contact angle the hydrodynamic resistance force reduces faster than the electrostatic force that drives the particle.

B. The interfacial deformation—electrodipping

On the basis of Eq. (24) there are, in general, two possible ways to deform the fluid interface due to the presence of the particle. However, we already showed in Sec. III B that the motion of the particle does not contribute to the interfacial deformation to first order in Ca. The only remaining contribution is called electrodipping [see Ref. 43]. Essentially, the sum of the Maxwell stress and the static pressure inside the EDL is balanced by the capillary pressure. In contrast to all published works concerning the electrodipping effect, we do not limit our analysis to the case of a small Debye length. However, in the present work the static interfacial deformation is independent of the

nonpolar fluid (as a consequence of assumption 4), as opposed to the theoretical works by Foret and Würger [42], Danov *et al.* [43], Danov and Kralchevsky [44], and Danov *et al.* [45].

The solution procedure is straightforward, since we provided the solution of the equilibrium potential $\bar{\psi}$ for a flat interface up to first order in the perturbation parameter β [see Eqs. (B4) and (B11) in Appendix B]. Consequently, the only task to calculate the stresses acting on the fluid interface is to solve Eq. (10) for the remaining unknown quantity $\bar{p}^{\mathrm{s}}$:

$$-\bar{\nabla}\bar{p}^{\mathrm{s}} + \bar{\nabla}^2\bar{\psi}\,\bar{\nabla}\bar{\psi} = -\bar{\nabla}\bar{p}^{\mathrm{s}} + (\kappa a)^2\bar{\psi}\,\bar{\nabla}\bar{\psi} = \bar{\nabla}\left(-\bar{p}^{\mathrm{s}} + \frac{(\kappa a)^2}{2}\bar{\psi}^2\right) = 0. \tag{36}$$

Taking the boundary conditions [Eq. (15)] into account leads to

$$\bar{p}^{\mathrm{s}} = \frac{(\kappa a)^2}{2}\bar{\psi}^2. \tag{37}$$

The reader should keep in mind that the left-hand side of Eq. (24) needs to be evaluated at the undeformed flat fluid interface, which suggests changing the coordinate system for the quantification of the interfacial deformation to cylindrical coordinates $(\bar{\rho}, \vartheta, \bar{x})$, following Dörr and Hardt [60]. The cylindrical coordinates are defined by

$$\bar{\rho} = \sqrt{\bar{y}^2 + \bar{z}^2}, \tag{38}$$

$$\vartheta = \theta + \frac{\pi}{2}. \tag{39}$$

In the static situation the EDL is axisymmetric around the particle, consequently, the interface deformation is as well. We introduce a function $\bar{h}$ denoting the height of the interface as follows:

$$\bar{x} = \bar{h}(\bar{\rho}). \tag{40}$$

We expand $\bar{h}(\bar{\rho})$ in powers of Ce, leading to $\bar{h}(\bar{\rho}) = \mathrm{Ce}\,\bar{\mathfrak{h}}(\bar{\rho}) + O(\mathrm{Ce}^2)$ and omit all terms higher than first order. The corresponding normal vector reads

$$\boldsymbol{n} = \boldsymbol{e}_x - \mathrm{Ce}\,\frac{\partial\bar{\mathfrak{h}}(\bar{\rho})}{\partial\bar{\rho}}\boldsymbol{e}_\rho + O(\mathrm{Ce}^2), \tag{41}$$

and therefore we obtain

$$\bar{\nabla}\cdot\boldsymbol{n} = -\left[\frac{1}{\bar{\rho}}\frac{\partial}{\partial\bar{\rho}}\left(\bar{\rho}\frac{\partial\bar{\mathfrak{h}}}{\partial\bar{\rho}}\right)\right]. \tag{42}$$

The equation for the interfacial deformation then reads

$$-\bar{p}^{\mathrm{s}} + \bar{M}^s_{\varphi\varphi} = -\left[\frac{1}{\bar{\rho}}\frac{\partial}{\partial\bar{\rho}}\left(\bar{\rho}\frac{\partial\bar{\mathfrak{h}}}{\partial\bar{\rho}}\right)\right]. \tag{43}$$

The $\varphi\varphi$ component of $\bar{\mathbf{M}}^s$ can be evaluated up to first order in β:

$$\bar{M}^s_{\varphi\varphi} = -\frac{1}{2}\left(\frac{\partial\bar{\psi}_{(0)}}{\partial\bar{r}}\right)^2 - \beta\,\frac{\partial\bar{\psi}_{(0)}}{\partial\bar{r}}\frac{\partial\bar{\psi}_{(1)}}{\partial\bar{r}} + O(\beta^2). \tag{44}$$

Accordingly, Eq. (37) leads to

$$\bar{p}^{\mathrm{s}} = \frac{(\kappa a)^2}{2}(\bar{\psi}_{(0)})^2 + \beta\,(\kappa a)^2\,\bar{\psi}_{(0)}\,\bar{\psi}_{(1)} + O(\beta^2). \tag{45}$$

1. $\Theta = 90°$—Zeroth-order solution

After inserting Eqs. (44) and (45) into Eq. (43), we find for the zeroth-order perturbation in β ($\Theta = 90°$):

$$\frac{1}{2}\left[(\kappa a)^2(\bar{\psi}_{(0)})^2 + \left(\frac{\partial \bar{\psi}_{(0)}}{\partial \bar{\rho}}\right)^2\right]\Bigg|_{\varphi=\frac{\pi}{2},\frac{3\pi}{2}} = \frac{1}{\bar{\rho}}\frac{\partial}{\partial \bar{\rho}}\left(\bar{\rho}\frac{\partial \bar{\mathfrak{h}}_{(0)}}{\partial \bar{\rho}}\right). \tag{46}$$

In Appendix D, we show (similarly to Danov and Kralchevsky [44]) that the solution of Eq. (46) can be written as

$$\bar{\mathfrak{h}}_{(0)}(\bar{\rho}) = \int_{\bar{\rho}}^{\infty} \ln\left(\frac{\tilde{\rho}}{\bar{\rho}}\right)\frac{\tilde{\rho}}{2}\left[(\kappa a)^2(\bar{\psi}_{(0)})^2 + \left(\frac{\partial \bar{\psi}_{(0)}}{\partial \tilde{\rho}}\right)^2\right]\Bigg|_{\varphi=\frac{\pi}{2},\frac{3\pi}{2}} d\tilde{\rho}. \tag{47}$$

For the transformation in the Appendix, we assumed the fluid interface to be flat far away from the particle. Equation (47) can be solved analytically, leading to

$$\bar{\mathfrak{h}}_{(0)}(\bar{\rho}) = \frac{\exp[-2\kappa a(\bar{\rho}-1)][1 + 2\kappa a\,\bar{\rho} + 4\exp(2\kappa a\,\bar{\rho})(\kappa a)^2\,\bar{\rho}^2\mathsf{Ei}(-2\kappa a\,\bar{\rho})]}{8\bar{\rho}^2}. \tag{48}$$

2. $O(\beta)$—First-order solution

The equation for the interfacial deformation to first order in the perturbation parameter β reads

$$\bar{\mathfrak{h}}_{(1)}(\bar{\rho}) = \int_{\bar{\rho}}^{\infty} \ln\left(\frac{\tilde{\rho}}{\bar{\rho}}\right)\tilde{\rho}\left[(\kappa a)^2\,\bar{\psi}_{(0)}\,\bar{\psi}_{(1)} + \frac{\partial \bar{\psi}_{(0)}}{\partial \tilde{\rho}}\frac{\partial \bar{\psi}_{(1)}}{\partial \tilde{\rho}}\right]\Bigg|_{\varphi=\frac{\pi}{2},\frac{3\pi}{2}} d\tilde{\rho}. \tag{49}$$

After transforming the integrand (see Appendix E) we obtain

$$\bar{\mathfrak{h}}_{(1)}(\bar{\rho}) = \int_{\bar{\rho}}^{\infty} \left[\ln\left(\frac{\tilde{\rho}}{\bar{\rho}}\right) - 1\right]\frac{\partial \bar{\psi}_{(0)}}{\partial \tilde{\rho}}\,\bar{\psi}_{(1)}\Bigg|_{\varphi=\frac{\pi}{2},\frac{3\pi}{2}} d\tilde{\rho}. \tag{50}$$

It is known that solutions of elliptic partial differential equations take their extremal values at the boundary of the domain (maximum principle) [see, e.g., Ref. 66]. The boundaries of $\bar{\psi}_{(1)}$ to be considered here are $\bar{\rho} = 1$ and $\bar{\rho} \to \infty$. The far-field behavior of the equilibrium electrostatic potential is controlled by the condition of vanishing potential at infinity [see Eq. (B9)]. Moreover, the boundary condition at $\bar{\rho} = 1$ reads

$$(\bar{\psi}_{(1)}|_{\bar{r}=1})|_{\varphi=\frac{\pi}{2},\frac{3\pi}{2}} = (1+\kappa a)\left\{\sum_{l=0}^{\infty} \mathsf{SH}_l[f(\theta,\varphi)]\right\}\Bigg|_{\varphi=\frac{\pi}{2},\frac{3\pi}{2}} \tag{51}$$

$$= (1+\kappa a)f(\theta,\varphi)|_{\varphi=\frac{\pi}{2},\frac{3\pi}{2}}. \tag{52}$$

Since $f(\theta,\frac{\pi}{2}) = f(\theta,\frac{3\pi}{2}) = 0$, $\bar{\psi}_{(1)}$ is identically zero at the boundaries and therefore zero everywhere at the undeformed interface. As a consequence, the $O(\beta)$ correction to the interfacial deformation vanishes:

$$\bar{\mathfrak{h}}_{(1)} = 0. \tag{53}$$

Figure 4 shows the resulting interfacial deformation up to $O(\beta)$ for different values of the Debye length [see Eq. (48) with $\bar{h}(\bar{\rho}) = \mathrm{Ce}\,\bar{\mathfrak{h}}(\bar{\rho}) + O(\mathrm{Ca}^2, \mathrm{Ce}^2, \beta^2)$]. In agreement with physical intuition, the deformation of the fluid interface strongly depends on the thickness of the EDL. In the Smoluchowski limit ($\kappa a \to \infty$), the interfacial deformation occurs on a very short length scale, as already suggested by Foret and Würger [42] and Danov *et al.* [43]. For real fluids with a permittivity ratio which is no longer small and for small values of the Debye length, this contribution only affects the interfacial deformation in close proximity of the particle, whereas the long-range deformation is dominated by the force distribution inside the nonpolar fluid. The
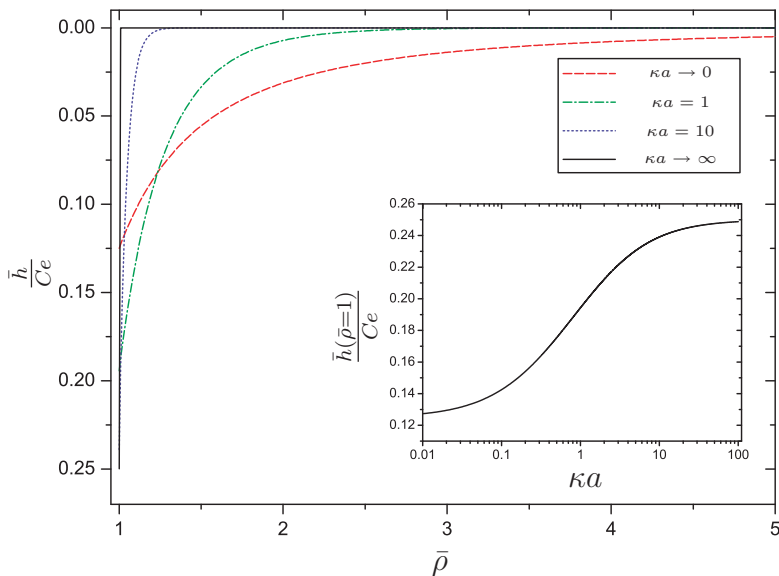
FIG. 4. Plot of the first-order interfacial deformation $\frac{\bar{h}(\bar{\rho})}{Ce} = \bar{\mathfrak{h}}$ (in Ce) over the dimensionless distance $\bar{\rho}$ for different values of the dimensionless Debye length [see Eq. (48)]. Inset: Dipping depth [see Eq. (54)] of the particle as a function of the Debye length.

interfacial deformation due to the charges at the particle-nonpolar fluid boundary is shown to scale like $\bar{h} \propto \bar{\rho}^{-4}$ [see Refs. 41,42,44,47], which is clearly a longer-range deformation as found in our study for $\kappa a \to \infty$. But, in case of a thick EDL, we obtain from Eq. (48) $\bar{h} = \frac{Ce}{8\bar{\rho}^2}$ (see Appendix F), which is a longer-range deformation than in the opposite case of a thin EDL. As the results by Foret and Würger [42] are valid at large distances, a superposition of both expressions would be suitable to take both the short-range and long-range interfacial deformations into account.

Since the gradient of the equilibrium potential $\bar{\psi}$ is linked to the force acting on the particle, it is evident that the dipping depth decreases with an increasing Debye length. The dipping depth of the particle can be found according to

$$\bar{h}(\bar{\rho} = 1) = \frac{Ce}{8}[1 + 2\kappa a + 4\exp(2\kappa a)(\kappa a)^2 \mathsf{Ei}(-2\kappa a)] + O(Ca^2, Ce^2, \beta^2). \tag{54}$$

The curve corresponding to Eq. (54) is shown in the inset of Fig. 4. The two limiting values can be found via

$$\lim_{\kappa a \to 0} \bar{h}(\bar{\rho} = 1) = \frac{Ce}{8} + O(Ca^2, Ce^2, \beta^2), \quad \lim_{\kappa a \to \infty} \bar{h}(\bar{\rho} = 1) = \frac{Ce}{4} + O(Ca^2, Ce^2, \beta^2). \tag{55}$$

V. DISCUSSION

A. Impact of the static interfacial deformation on the electrophoretic mobility

In this section we aim at making some predictions about the influence of the interfacial deformation on the electrophoretic mobility of particles. We limit ourselves to small values of the Debye length.

In the foregoing section we obtained an analytical solution for the fluid interface deformation caused by the presence of a charged particle. In the case of a small Debye length, the deformation of the interface is limited to a region very close to the surface of the particle (see Fig. 4). In that case

($\kappa a \to \infty$), we can approximate the interface shape via

$$\bar{h}(\bar{\rho}) = \begin{cases} \frac{\text{Ce}}{4}, & \text{for } \bar{\rho} = 1 \\ 0, & \text{for } \bar{\rho} > 1 \end{cases}, \tag{56}$$

which is supposed to be valid up to first order of β, Ca, and Ce. From a physical point of view, Eq. (56) describes a small variation of the contact angle at the particle surface, while the fluid interface remains flat. The fact that the presence of an EDL modifies the apparent contact angle is of course known from the literature [49,67]. Consequently, up to first order in Ce, the electrophoretic mobility can be calculated by assuming a flat fluid interface and a modified contact angle Θ_{app}. Geometric considerations lead to

$$\Theta_{\text{app}} = \Theta - \frac{\text{Ce}}{4} + O(\beta^2, \text{Ce}^2). \tag{57}$$

This equation is valid up to first order in β, since the same is true for Eqs. (48) and (56). In the thin Debye layer limit, the contact angle at the surface of a charged particle decreases with increasing electric capillary number Ce. For example, for Ce $= 0.1$ and $\Theta = 90°$, the effective contact angle reaches $\Theta_{\text{app}} \approx 88.57°$. Based on such a scenario where only the contact angle gets modified, the Smoluchowski limit [see Eq. (26)] remains valid. Even at higher orders in Ce the physics of the problem suggests that the interface deformation only occurs in the upmost vicinity of the particle surface if the thin Debye layer limit applies. Therefore, in this limiting case the Smoluchowski expression for the electrophoretic mobility should remain valid as long as the assumption 4 is approximately valid.

B. Validity range of the theory for the electrophoretic mobility

In this subsection, we aim at testing the validity our theory for the electrophoretic mobility. Among others, we would like to quantify the errors introduced by limiting the description to a first-order perturbation around a contact angle of 90°.

We considered a weak applied electric field which allowed us to derive the present set of governing equations based on a perturbation approach around the equilibrium state. This results in a linear relationship between the particle velocity and the electric field; see Eq. (1). When the applied electric field is sufficiently strong, a second cloud of counterions (outside the EDL) is induced because of concentration polarization [54], leading to a third-order correction to the electrophoretic velocity, i.e.,

$$U = \eta^{(1)} E_\infty + \eta^{(3)} E_\infty^3 + O\left(E_\infty^5\right). \tag{58}$$

Apart from that, Barany [54] has presented experimental results to identify the range of validity of the weak-field approximation. Among others, graphite and $\gamma - \text{Al}_2\text{O}_3$ particles in high electric fields were studied and the weak-field approximation was found to be valid up to 50 V/cm and 200 V/cm, respectively, for thin Debye layers.

Our second assumption, i.e., a small ζ potential, has been widely discussed in the literature already shortly after the first theoretical works on electrophoresis appeared, especially after the publication of Henry [11]. Large ζ potentials cause a reduction of the velocity of a particle for moderate Debye parameters $0.2 < \kappa a < 50$ [7]. In the numerical work of Wiersema *et al.* [16], the authors found the highest discrepancy between the linear theory of Henry [11] and their results to occur at $\kappa a \approx 5$. At this value of the Debye parameter, they showed that the linear theory is valid up to $\bar{\zeta} := \frac{e\zeta}{k_B T} \approx 1.5$ or $\zeta \approx 37$ mV at room temperature. For different values of κa the range of validity increases. $\zeta \approx 37$ mV is a value that still includes the range of ζ potentials of many materials [see, e.g., Ref. 68].

We expect that these results on the validity of the weak-field approximation and the assumption concerning the ζ potential can be largely transferred to the case of interfacial particles. This is due to
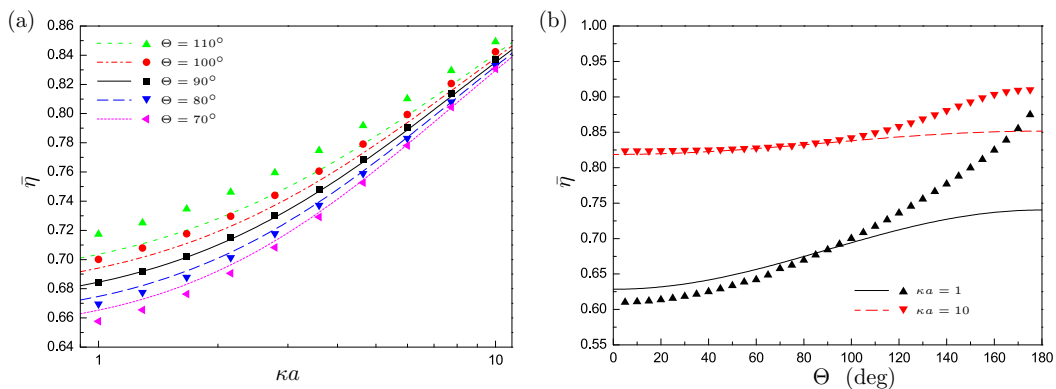
FIG. 5. Comparison between the numerical results and the predictions of the theory. (a) Electrophoretic mobility as a function of the Debye parameter obtained with Eqs. (32) and (34) for different contact angles compared to numerical solutions. The lines indicate the analytical, the symbols the numerical results. (b) Electrophoretic mobility as a function of the contact angle for two different values of the Debye parameter. The lines indicate the analytical, the symbols the numerical results.

the fact that the scenario of electrophoretic transport of a spherical particle in the bulk is contained in our analysis as the special case of a flat fluid interface and a contact angle of $90°$.

We calculated the electrophoretic mobility of spherical interfacial particles up to first order in the deviation of the contact angle from $90°$. The range of contact angles that is fairly well approximated by our theory is a priori unknown. To check the validity of the first-order approximation, we used the commercial finite-element solver COMSOL Multiphysics [69] to solve the set of governing equations, described in more detail in Appendix G. The comparison between the theoretical model and the numerical simulations is shown in Fig. 5. In Fig. 5(a), the electrophoretic mobility is plotted against the Debye parameter for different contact angles around $90°$. The model clearly predicts the electrophoretic mobility of hydrophilic particles better than that of hydrophobic ones. Over the whole range of contact angles considered, the maximum discrepancy between the numerical results and our model is found to be within 4%. To capture the dependency of the mobility on the contact angle over a broader range, simulations for two specific values of the Debye parameter were performed. The plot in Fig. 5(b) supports the insights from Fig. 5(a). In general, the theory is found to be more accurate for thin EDLs. Interestingly, the theory is still accurate even for very small contact angles. The deviation between the theoretical and the simulation results is found to be smaller than 4% even for $\Theta = 5°$, while the deviations between theory and simulations become larger for hydrophobic particles. However, when defining the range of validity of the theory by demanding deviations of less than 5% from the simulation results, our theory is valid up to $\Theta = 130°$. This includes all conventional hydrophobic surfaces, but excludes superhydrophobic materials. We are therefore left with the conclusion that in terms of the contact angle the theory provides a good approximation to the electrophoretic mobility of almost all interfacial particles.

Before we illustrate a possible application of our model, we comment on some additional effects that might limit its applicability in the Hückel limit ($\kappa a \to 0$). In this case, the particle can be very small, making the effects of Brownian motion more prominent. While the same is true for particles in the bulk, the presence of the fluid interface introduces additional effects, i.e., the Brownian motion of the particle gives rise to capillary waves [see, e.g., Ref. 70]. Moreover, the relative surface roughness (compared to the size of the particle) of a small particle can be very significant, leading to a noncircular three-phase contact line at the particle surface. In this case, the zeroth-order solution does not yield a fluid-interface profile as considered in our model. The impact of these effects on the electrophoretic mobility of very small particles and the corresponding interfacial deformation it is yet to be explored.

C. Application: Separation of Janus particles

The purpose of this subsection is to illustrate a potential application related to the electrophoretic transport of interfacial particles. The application is based on spherical particles composed of two different hemispheres, so-called Janus particles. Janus particles have been intensely studied in recent years due to their various applications, e.g., in e-paper display technologies [71]. In this subsection, we discuss the differences in electrophoretic transport of Janus particles suspended in a bulk liquid and Janus particles attached to a fluid interface. Due to the different wetting properties of the two materials the particle consists of, an interfacial Janus particle will usually align itself at the interface in such a way that only one hemisphere is immersed in the electrolyte solution [e.g., Refs. 72,73]. In this case, the electrophoretic mobility of the particle is equal to that of a homogeneous particle having the same ζ potential and contact angle as the immersed part of the Janus particle. However, Janus particles suspended in the bulk of a liquid behave differently. The theoretical framework for the electrophoretic motion of Janus particles in the bulk is included in the work by Kim and Yoon [53]. In the following, we briefly discuss the electrophoretic mobility and the particle alignment in the bulk, to point out the differences to a Janus particle attached to a fluid interface.

We consider a ζ-potential distribution around the particle according to

$$\zeta(\theta) = \begin{cases} \zeta_0, & \text{for } 0 < \theta \leqslant \frac{\pi}{2} \\ \alpha\,\zeta_0, & \text{for } \frac{\pi}{2} < \theta \leqslant \pi \end{cases}, \quad \text{with } -1 \leqslant \alpha \leqslant 1. \tag{59}$$

Following Kim and Yoon [53], the ζ-potential distribution has to be expanded in terms of the first three ($l = 0, 1, 2$) spherical harmonics, according to Appendix C, since higher-order terms do not contribute to the electrophoretic mobility. Further, the terms with $l = 0$ and $l = 2$ solely contribute to the translational mobility, whereas $l = 1$ influences the rotation of the particle, i.e., the alignment with the electric field. After some calculation, the translational electrophoretic mobility is found to be

$$\bar{\eta}_{\text{Janus}} = \frac{1 + \alpha}{2} \bar{\eta}_0, \tag{60}$$

with $\bar{\eta}_0$ from Eq. (32). In other words, the electrophoretic mobility is identical to that of a homogeneous particle with the average value of the ζ potential, clearly in agreement with physical intuition. For $\alpha = -1$, the mobility vanishes. In this case, the particle will not exhibit any steady-state translation but align itself in the electric field through rotation. By contrast, if the particle gets attached to a fluid interface (under the assumptions formulated in Sec. II), its electrophoretic mobility is given by Eqs. (32) and (34), where the ζ potential of the hemisphere immersed in the electrolyte solution needs to be taken into account. This means that in contrast to the case of a fully immersed particle, an interfacial particle translates along the interface if $\zeta_0 \neq 0$. More generally, electrophoresis of particles attached to a fluid interface enables separation processes that are not possible in the bulk of a liquid. In the bulk, a Janus particle translates with a velocity corresponding to its average ζ potential, which makes the separation of different particles with the same average ζ potential impossible. Electrophoretic transport along a fluid interface, however, enables the separation of different Janus particles if only the ζ potentials of the hemispheres immersed in the electrolyte solution are different.

VI. CONCLUSION

In summary, we have studied the electrophoretic motion of a single neutrally buoyant particle attached to a fluid interface for vanishing viscosity and permittivity ratios. Along with that, the deformation of the fluid interface due to the Debye layer around the particle was analyzed. The analysis is based on combined perturbation expansions in the capillary number, the electric capillary number, and the deviation of the contact angle at the particle surface from $90°$. Assuming a small interfacial deformation, we found a generalization of the Smoluchowski mobility for particles of arbitrary shape. As a consequence, the Smoluchowski limit holds for spherical particles independently of the contact angle at the particle surface. The overall interfacial deformation

is a superposition of a dynamic (due to hydrodynamic stress) and a static (due to electrostatic stress) deformation. Assuming a mirror-symmetric shape of the particle with respect to the plane perpendicular to the direction of motion, we found that the motion of the particle (controlled by the capillary number Ca) does not contribute to the interfacial deformation, no matter what the Debye layer thickness is. To compute the electrophoretic mobility for arbitrary values of the Debye layer thickness, we considered a spherical particle with a contact angle in the vicinity of 90°. In the limiting case of thick Debye layers, hydrophobic particles have a higher electrophoretic mobility than hydrophilic ones. Further, the static interfacial deformation was computed. From the shape of the interface the dipping depth of the particle can be computed, taking values of $a\frac{\text{Ce}}{4}$ and $a\frac{\text{Ce}}{8}$ for thin and thick Debye layers, respectively, in which a denotes the radius of the spherical particle and Ce the electric capillary number. Our results indicate that even when gravity is neglected, a long-range capillary interaction between two particles (as observed from the experimental results in Nikolaides *et al.* [39] and Aveyard *et al.* [40]) is indeed possible if the Debye length is large compared to the particle radius. Moreover, we discussed the influence of the electrodipping effect on the electrophoretic mobility. In the case of a small Debye length it suggests itself that the Smoluchowski limit remains valid even for a deformed fluid interface, since the interface deformation is equivalent to a change in contact angle at the particle surface. We also examined the validity limits of our model. We especially considered the influence of strong applied fields, large ζ potentials and contact angle deviations from 90°. The influence of the contact angle was studied by comparing the analytical results to the results of numerical simulations for Debye parameters κa taking values between 1 and 10. For contact angles on the particle smaller than 130°, the maximum deviations between the analytical and the numerical results are limited to 5%, which leaves us with the conclusion that our theory is sufficiently accurate for almost all practically relevant contact angles.

The results may find applications in different contexts. First, they could help understanding the response of soft matter systems with interfacial particles such as Pickering emulsions or liquid marbles to electric fields. An overview of the response of particle-laden drops under electric fields was given by Dommersnes and Fossum [74]. For example, our analysis could be relevant for the electric-field induced coalescence of particle-covered water drops, as reported in Ref. [75]. Novel electrophoretic separation schemes constitute another potential application that was discussed in some detail in Sec. V C. Finally, the deformation of the fluid interface gives rise to a capillary interaction of interfacial particles, which will be the subject of future work.

APPENDIX A: THE DYNAMIC INTERFACIAL DEFORMATION, EQ. (28)

We define the abbreviation $\mathbf{I}(\bar{r}, \theta) := \bar{\boldsymbol{\sigma}} \cdot \boldsymbol{n}_I + \frac{1}{\bar{\eta}}\bar{\mathbf{M}}^d \cdot \boldsymbol{n}_I$ and expand Eq. (28) into

$$\mathfrak{T}_P = \int_0^\pi \int_{\bar{r}_P(\theta)}^\infty \bar{r}^2 \boldsymbol{e}_r \times \mathbf{I}(\bar{r}, \theta)|_{\varphi=\frac{\pi}{2},\frac{3\pi}{2}} \, d\bar{r} \, d\theta + \int_\pi^{2\pi} \int_{\bar{r}_P(\theta)}^\infty \bar{r}^2 \boldsymbol{e}_r \times \mathbf{I}(\bar{r}, \theta)|_{\varphi=\frac{\pi}{2},\frac{3\pi}{2}} \, d\bar{r} \, d\theta. \quad \text{(A1)}$$

The second integral can be transformed into

$$\int_\pi^{2\pi} \int_{\bar{r}_P(\theta)}^\infty \bar{r}^2 \boldsymbol{e}_r \times \mathbf{I}(\bar{r}, \theta)|_{\varphi=\frac{\pi}{2},\frac{3\pi}{2}} \, d\bar{r} \, d\theta = -\int_{2\pi}^\pi \int_{\bar{r}_P(\theta)}^\infty \bar{r}^2 \boldsymbol{e}_r \times \mathbf{I}(\bar{r}, \theta)|_{\varphi=\frac{\pi}{2},\frac{3\pi}{2}} \, d\bar{r} \, d\theta \quad \text{(A2)}$$

$$= -\int_0^{-\pi} \int_{\bar{r}_P(\theta)}^\infty \bar{r}^2 \boldsymbol{e}_r \times \mathbf{I}(\bar{r}, \theta)|_{\varphi=\frac{\pi}{2},\frac{3\pi}{2}} \, d\bar{r} d\theta \quad \text{(A3)}$$

$$= \int_0^{-\pi} \int_{\bar{r}_P(\theta)}^\infty \bar{r}^2 \boldsymbol{e}_r \times \mathbf{I}(\bar{r}, -\theta)|_{\varphi=\frac{\pi}{2},\frac{3\pi}{2}} \, d\bar{r} d\theta. \quad \text{(A4)}$$

For the step from Eqs. (A3) to (A4) we used $-\mathbf{I}(\bar{r}, \theta) = \mathbf{I}(\bar{r}, -\theta)$. By substituting $\chi = -\theta$, we find

$$\int_{\pi}^{2\pi} \int_{\bar{r}_P(\theta)}^{\infty} \bar{r}^2 \boldsymbol{e}_r \times \mathbf{I}(\bar{r}, \theta)|_{\varphi = \frac{\pi}{2}, \frac{3\pi}{2}} \, d\bar{r} \, d\theta = -\int_{0}^{\pi} \int_{\bar{r}_P(-\chi)}^{\infty} \bar{r}^2 \boldsymbol{e}_r \times \mathbf{I}(\bar{r}, \chi)|_{\varphi = \frac{\pi}{2}, \frac{3\pi}{2}} \, d\bar{r} d\chi. \quad \text{(A5)}$$

Since a mirror-symmetric particle with respect to the plane perpendicular to its motion is assumed, $\bar{r}_P(\theta)$ is an even function $[\bar{r}_P(\theta) = \bar{r}_P(-\theta)]$, and Eq. (28) is identically zero.

APPENDIX B: SOLUTION OF THE GOVERNING EQUATIONS

1. $\Theta = 90°$—Zeroth-order solution

The zeroth-order solution corresponds to an undeformed sphere in an unbounded fluid. Under the assumptions made, this is equivalent to the case studied by Henry [11]. Instead of going through this quite cumbersome mathematics, and to simplify the calculations for the first order in β, we utilize Teubner's method [14]. By a generalization of the reciprocal theorem for Stokes flow [see Ref. 76], and by comparing a charged and an uncharged state of the particle, he found that the Stokes equations with a source term corresponding to the electrostatic force are no longer needed to be solved analytically. Instead, the nondimensional force balance at the particle surface can be rewritten into [see Ref. 14]

$$\bar{\eta} = -\frac{\int_V [\bar{\nabla}^2 \bar{\psi} \bar{\nabla} \bar{\phi} \cdot (\bar{\boldsymbol{v}}^c - \boldsymbol{e}_z)] \, dV}{\int_{\Gamma_P} \bar{\boldsymbol{\sigma}}^c|_{\bar{r}=1} \cdot \boldsymbol{n}^P \cdot \boldsymbol{e}_z \, dS}, \quad \text{(B1)}$$

in which $\bar{\boldsymbol{v}}^c$ and $\bar{\boldsymbol{\sigma}}^c$ correspond to the Stokes equations without source term. The solutions of the homogeneous Stokes equations, as well as the solutions of the Laplace and Poisson-Boltzmann equations, satisfying the boundary condition Eqs. (15) and (16), are readily known [see Refs. 14,77]:

$$\bar{\boldsymbol{v}}_{(0)}^c = -\tfrac{1}{2} \cos(\theta)(\bar{r}^{-3} - 3\bar{r}^{-1})\boldsymbol{e}_r - \tfrac{1}{4} \sin(\theta)(\bar{r}^{-3} + 3\bar{r}^{-1})\boldsymbol{e}_\theta, \quad \text{(B2)}$$

$$\bar{p}_{(0)}^c = \tfrac{3}{2} \cos(\theta)\bar{r}^{-2}, \quad \text{(B3)}$$

$$\bar{\psi}_{(0)} = \exp[-\kappa a(\bar{r} - 1)]\bar{r}^{-1}, \quad \text{(B4)}$$

$$\bar{\phi}_{(0)} = -\cos(\theta)(\bar{r} + \tfrac{1}{2}\bar{r}^{-2}). \quad \text{(B5)}$$

Inserting Eqs. (B2)–(B5) into Eq. (B1) leads to the famous result by Henry [11] as given in Eq. (32).

2. $O(\beta)$—First-order solution

As already mentioned in Sec. IV A, the zeroth-order solutions [Eqs. (B2)–(B5)] from the foregoing paragraph are the basis for the first-order perturbation solutions in β. This is due to the fact that the boundary conditions on the deformed sphere are mapped to an undeformed one. The first-order solution of the Stokes equation without source term is available from Brenner [61] and has already been utilized by Dörr and Hardt [60] for the representation of the particle shape given in Eq. (30). We omit the derivation of the corresponding solution and refer the reader to Brenner [61] and Dörr and Hardt [60]. Instead, we focus on the solutions of the Laplace and linearized Poisson-Boltzmann equations. First, we map the boundary conditions on the undeformed sphere by

applying a Taylor expansion around $\bar{r} = 1$ and find

$$\bar{\psi}_{(1)}|_{\bar{r}=1} = -f(\theta, \varphi) \frac{\partial \bar{\psi}_{(0)}}{\partial \bar{r}}\bigg|_{\bar{r}=1} = (1 + \kappa a) f(\theta, \varphi), \tag{B6}$$

$$\frac{\partial \bar{\phi}_{(1)}}{\partial \bar{r}}\bigg|_{\bar{r}=1} = -f(\theta, \varphi) \frac{\partial^2 \bar{\phi}_{(0)}}{\partial \bar{r}^2}\bigg|_{\bar{r}=1} + \nabla \bar{\phi}_{(0)}|_{\bar{r}=1} \cdot \nabla f(\theta, \varphi)$$

$$= \frac{9}{2} \cos(\theta) f(\theta, \varphi). \tag{B7}$$

Following Brenner [61], the right-hand sides of Eqs. (B6) and (B7) need to be expanded in terms of spherical harmonics [see Refs. 56,64,65]. In the following, we denote $\mathsf{SH}_l(\varsigma(\theta, \varphi))$ the lth partial sum of the expansion of $\varsigma(\theta, \varphi) = \sum_{l=0}^{\infty} \mathsf{SH}_l(\varsigma(\theta, \varphi))$ (see Appendix C). Consequently, we assume solutions of both equations of the following forms:

$$\bar{\psi}_{(1)} = \sum_{l=0}^{\infty} \bar{\psi}_{(1)}^{(l)}, \quad \bar{\phi}_{(1)} = \sum_{l=0}^{\infty} \bar{\phi}_{(1)}^{(l)}. \tag{B8}$$

Every partial sum of Eq. (B8) has to satisfy the corresponding governing equation together with the boundary conditions

$$\bar{\psi}_{(1)}^{(l)}\big|_{\bar{r}=1} = (1 + \kappa a) \mathsf{SH}_l(f(\theta, \varphi)), \quad \bar{\psi}_{(1)}^{(l)}\big|_{\bar{r}\to\infty} = 0, \tag{B9}$$

$$\frac{\partial \bar{\phi}_{(1)}^{(l)}}{\partial \bar{r}}\bigg|_{\bar{r}=1} = \frac{9}{2} \mathsf{SH}_l(\cos(\theta) f(\theta, \varphi)), \quad \bar{\phi}_{(1)}^{(l)}\big|_{\bar{r}\to\infty} = 0. \tag{B10}$$

The first five partial sums of Eqs. (B9) and (B10) are given in Appendix C.

The solutions of the Laplace and Poisson-Boltzmann equations are available for the given set of boundary conditions [see Ref. 53]. Translated to our notation they read

$$\bar{\psi}_{(1)}^{(l)} = (1 + \kappa a) \bar{r}^{-(l+1)} \exp(-\kappa a(\bar{r} - 1)) \frac{\mathsf{K}_l(\kappa a \bar{r})}{\mathsf{K}_l(\kappa a)} \mathsf{SH}_l(f(\theta, \varphi)), \tag{B11}$$

with

$$\mathsf{K}_l(x) = \sum_{s=0}^{l} \frac{2^s l!(2l-s)!}{s!(2l)!(l-s)!} x^s, \tag{B12}$$

$$\bar{\phi}_{(1)}^{(l)} = -\frac{9}{2} \frac{1}{(l+1)} \bar{r}^{-(l+1)} \mathsf{SH}_l(\cos(\theta) f(\theta, \varphi)). \tag{B13}$$

Again, using Eq. (B1) we obtain the first-order electrophoretic mobility coefficient as given in Eq. (34).

APPENDIX C: EXPANSION OF A FUNCTION IN TERMS OF SPHERICAL HARMONICS

In this Appendix, we give a brief instruction into the expansion of an arbitrary function $f(\theta, \varphi)$ into a series of spherical harmonics. We therefore reproduce the results of Byerly [64], MacRobert [65], and Jackson [56]. Spherical harmonics are defined as

$$Y_{lm}(\theta, \varphi) = \sqrt{\frac{2l+1}{4\pi} \frac{(l-m)!}{(l+m)!}} P_l^m[\cos(\theta)] \exp(im\varphi), \tag{C1}$$

with $P_l^m(x)$ being the associated Legendre function and i the imaginary unit. Due to the orthogonality and completeness properties of spherical harmonics, any sufficiently smooth function $f(\theta, \varphi)$ can be expanded in terms of these functions. As short-hand notation we define $\chi = \cos(\theta)$ and expand $f(\chi, \varphi)$ via

$$A_{0,l} = \frac{2l+1}{4\pi} \int_0^{2\pi} \int_{-1}^1 f(\chi, \varphi) P_l(\chi) d\chi \, d\varphi, \tag{C2}$$

$$A_{m,l} = \frac{2l+1}{2\pi} \frac{(l-m)!}{(l+m)!} \int_0^{2\pi} \int_{-1}^1 f(\chi, \varphi) \cos(m\varphi) P_l^m(\chi) d\chi \, d\varphi, \tag{C3}$$

$$B_{m,l} = \frac{2l+1}{2\pi} \frac{(l-m)!}{(l+m)!} \int_0^{2\pi} \int_{-1}^1 f(\chi, \varphi) \sin(m\varphi) P_l^m(\chi) d\chi \, d\varphi, \tag{C4}$$

$$\mathsf{SH}_l(f(\chi, \varphi)) = A_{0,l} P_l(\chi) + \sum_{m=1}^l \left(A_{m,l} \cos(m\varphi) + B_{m,l} \sin(m\varphi) \right) P_l^m(\chi). \tag{C5}$$

Therefore, Eq. (B9), with $f_1(\chi, \varphi) = \sqrt{1-\chi^2}|\cos(\varphi)|$, leads to

$$\mathsf{SH}_0(f_1(\chi, \varphi)) = \frac{1}{2}, \tag{C6}$$

$$\mathsf{SH}_2(f_1(\chi, \varphi)) = -\frac{5}{32}[-1 + 3\chi^2 + 3(\chi^2 - 1)\cos(2\varphi)], \tag{C7}$$

$$\mathsf{SH}_4(f_1(\chi, \varphi)) = -\frac{3[9 - 90\chi^2 + 105\chi^4 + 20(1 - 8\chi^2 + 7\chi^4)\cos(2\varphi)]}{1024}$$
$$- \frac{105[(\chi^2 - 1)^2 \cos(4\varphi)]}{1024}, \tag{C8}$$

$$\vdots$$

Note that all $\mathsf{SH}_j(f_1(\chi, \varphi))$, with $j = 2l - 1$, vanish, since $f_1(\chi, \varphi)$ is even with respect to χ. Following the same procedure, Eq. (B10), with $f_2(\chi, \varphi) = \chi\sqrt{1-\chi^2}|\cos(\varphi)|$, leads to

$$\mathsf{SH}_1(f_2(\chi, \varphi)) = \frac{3\chi}{8}, \tag{C9}$$

$$\mathsf{SH}_3(f_2(\chi, \varphi)) = -\frac{7}{64}\chi[-3 + 5\chi^2 + 5(\chi^2 - 1)\cos(2\varphi)], \tag{C10}$$

$$\mathsf{SH}_5(f_2(\chi, \varphi)) = -\frac{55\chi[15 - 70\chi^2 + 63\chi^4 + 28(1 - 4\chi^2 + 3\chi^4)\cos(2\varphi)]}{8192}$$
$$- \frac{1155\chi(\chi^2 - 1)^2 \cos(4\varphi)}{8192}, \tag{C11}$$

$$\vdots$$

Here, $\mathsf{SH}_j(f_2(\chi, \varphi)) = 0$, if $j = 2l$, since $f_2(\chi, \varphi)$ is odd with respect to χ.

APPENDIX D: SOLUTION OF DIFFERENTIAL EQUATIONS SIMILAR TO EQ. (46)

We consider an ordinary differential equation of the type

$$\frac{1}{r} \frac{\partial}{\partial r} \left(r \frac{\partial f(r)}{\partial r} \right) = g(r), \tag{D1}$$

with $g(r)$ and $f(r)$ fulfilling $\lim_{r \to \infty} g(r) = 0$, $\lim_{r \to \infty} f(r) = 0$ and $\lim_{r \to \infty} \frac{\partial f(r)}{\partial r} = 0$. Equation (D1) can be transformed into

$$\left[r \frac{\partial f(r)}{\partial r} \right]_{\rho}^{\infty} = \int_{\rho}^{\infty} r g(r) dr,$$

$$\frac{\partial f(\rho)}{\partial \rho} = -\frac{1}{\rho} \int_{\rho}^{\infty} r g(r) dr,$$

$$f(\tilde{\rho}) = \int_{\tilde{\rho}}^{\infty} \frac{1}{\rho} \int_{\rho}^{\infty} r g(r) dr d\rho.$$

We define $\xi(\rho) = \frac{1}{\rho}$ and $\chi(\rho) = \int_{\rho}^{\infty} r g(r) dr$ and apply the Leibniz integral theorem to find

$$\frac{\partial \chi(\rho)}{\partial \rho} = -\rho \, g(\rho),$$

and by partial integration

$$\int_{\tilde{\rho}}^{\infty} \frac{1}{\rho} \int_{\rho}^{\infty} r g(r) dr d\rho = \left[\ln(\rho) \int_{\rho}^{\infty} r g(r) dr \right]_{\tilde{\rho}}^{\infty} + \int_{\tilde{\rho}}^{\infty} \ln(\rho) \rho g(\rho) d\rho$$

$$= -\ln(\tilde{\rho}) \int_{\tilde{\rho}}^{\infty} r g(r) dr + \int_{\tilde{\rho}}^{\infty} \ln(\rho) \rho g(\rho) d\rho$$

$$\Rightarrow \quad f(\tilde{\rho}) = \int_{\tilde{\rho}}^{\infty} \ln \left(\frac{\rho}{\tilde{\rho}} \right) \rho g(\rho) d\rho. \tag{D2}$$

APPENDIX E: ALTERNATIVE FORM OF THE INTEGRAND IN EQ. (49)

The second part of the integrand in Eq. (49) can be rewritten (via the product rule) as

$$(\kappa a)^2 \bar{\psi}_{(0)} \bar{\psi}_{(1)} + \frac{\partial \bar{\psi}_{(0)}}{\partial \rho} \frac{\partial \bar{\psi}_{(1)}}{\partial \rho} = \left[(\kappa a)^2 \bar{\psi}_{(0)} - \frac{\partial^2 \bar{\psi}_{(0)}}{\partial \rho^2} \right] \bar{\psi}_{(1)} + \frac{\partial}{\partial \rho} \left[\frac{\partial \bar{\psi}_{(0)}}{\partial \rho} \bar{\psi}_{(1)} \right],$$

and further by replacing $(\kappa a)^2 \bar{\psi}_{(0)}$ using Eq. (13):

$$\left[(\kappa a)^2 \bar{\psi}_{(0)} - \frac{\partial^2 \bar{\psi}_{(0)}}{\partial \rho^2} \right] \bar{\psi}_{(1)} + \frac{\partial}{\partial \rho} \left[\frac{\partial \bar{\psi}_{(0)}}{\partial \rho} \bar{\psi}_{(1)} \right] = \frac{2}{\rho} \frac{\partial \bar{\psi}_{(0)}}{\partial \rho} \bar{\psi}_{(1)} + \frac{\partial}{\partial \rho} \left[\frac{\partial \bar{\psi}_{(0)}}{\partial \rho} \bar{\psi}_{(1)} \right].$$

Inserting this into Eq. (47) leads to

$$\bar{\mathfrak{h}}_{(1)}(\tilde{\rho}) = \int_{\tilde{\rho}}^{\infty} \ln \left(\frac{\rho}{\tilde{\rho}} \right) \rho \left[\frac{2}{\rho} \frac{\partial \bar{\psi}_{(0)}}{\partial \rho} \bar{\psi}_{(1)} + \frac{\partial}{\partial \rho} \left(\frac{\partial \bar{\psi}_{(0)}}{\partial \rho} \bar{\psi}_{(1)} \right) \right] \Bigg|_{\varphi = \frac{\pi}{2}, \frac{3\pi}{2}} d\rho. \tag{E1}$$

The integral of the second term in brackets is given by

$$I = \int_{\tilde{\rho}}^{\infty} \ln \left(\frac{\rho}{\tilde{\rho}} \right) \rho \left[\frac{\partial}{\partial \rho} \left(\frac{\partial \bar{\psi}_{(0)}}{\partial \rho} \bar{\psi}_{(1)} \right) \right] \Bigg|_{\varphi = \frac{\pi}{2}, \frac{3\pi}{2}} d\rho.$$
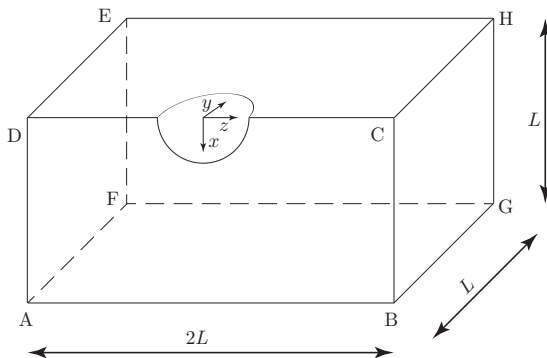
FIG. 6. Computational domain used in the COMSOL Multiphysics simulations.

By partial integration we obtain

$$
I = \left[\ln\left(\frac{\rho}{\tilde{\rho}}\right) \rho \frac{\partial \bar{\psi}_{(0)}}{\partial \rho} \bar{\psi}_{(1)} \bigg|_{\varphi=\frac{\pi}{2},\frac{3\pi}{2}} \right]_{\tilde{\rho}}^{\infty} - \int_{\tilde{\rho}}^{\infty} \left[1 + \ln\left(\frac{\rho}{\tilde{\rho}}\right) \right] \frac{\partial \bar{\psi}_{(0)}}{\partial \rho} \bar{\psi}_{(1)} \bigg|_{\varphi=\frac{\pi}{2},\frac{3\pi}{2}} d\rho.
$$

Inserting the boundary conditions for the equilibrium potential makes the first term vanish. Inserting the result into Eq. (E1) finally leads to

$$
\bar{\mathfrak{h}}_{(1)}(\tilde{\rho}) = \int_{\tilde{\rho}}^{\infty} \left[\ln\left(\frac{\rho}{\tilde{\rho}}\right) - 1 \right] \frac{\partial \bar{\psi}_{(0)}}{\partial \rho} \bar{\psi}_{(1)} \bigg|_{\varphi=\frac{\pi}{2},\frac{3\pi}{2}} d\rho. \tag{E2}
$$

APPENDIX F: INTERFACIAL DEFORMATION IN THE LIMIT OF THICK EDLs, $\kappa a \to 0$

We may examine the asymptotic interfacial deformation for thick EDL according to Eq. (48) by utilizing a Taylor expansion around $\kappa a = 0$. Apart from the well-known Taylor expansions of the exponential functions appearing in Eq. (48), we find for the exponential integral function

$$
\mathsf{Ei}(-2\,\kappa a\,\bar{\rho}) = \gamma_{\mathsf{E}} + \ln(2\,\kappa a\,\bar{\rho}) + \sum_{n=1}^{\infty} \frac{(-2\,\bar{\rho})^n}{n n!}(\kappa a)^n. \tag{F1}
$$

$\gamma_{\mathsf{E}} \approx 0.577$ is the Euler-Mascheroni constant. In Eq. (48) the exponential integral function is multiplied by $(\kappa a)^2$ and therefore only contributes to the second order of κa. Up to first order we find the expansion

$$
\bar{\mathfrak{h}}_{(1)}(\bar{\rho}) = \frac{1}{8\bar{\rho}^2} + \frac{\kappa a}{4\bar{\rho}^2} + O(\kappa a)^2, \tag{F2}
$$

which consequently leads to

$$
\lim_{\kappa a \to 0} \bar{\mathfrak{h}}_{(1)}(\bar{\rho}) = \frac{1}{8\bar{\rho}^2}. \tag{F3}
$$

APPENDIX G: DETAILS OF THE NUMERICAL SIMULATIONS USING COMSOL MULTIPHYSICS

Our theoretical model is derived based on a perturbation in the contact angle on the surface of the spherical interfacial particle. To evaluate the range of validity in this context, we employed numerical simulations using the commercial finite-element tool COMSOL Multiphysics [69]. Since our numerical scheme is inspired by the procedure described in Masliyah and Bhattacharjee [77], we avoid going into too much detail and just briefly discuss the method employed. Consistent with

TABLE I. Boundary conditions corresponding to Fig. 6.

Boundary	Variable	Description	Expression
Particle surface	$\bar{\boldsymbol{v}}$	No slip	$\bar{\boldsymbol{v}} = \boldsymbol{0}$
	$\bar{\psi}$	Dirichlet	$\bar{\psi} = 1$
	$\bar{\phi}$	Zero gradient	$\boldsymbol{n} \cdot \bar{\nabla}\bar{\phi} = 0$
A-D-E-F	$\bar{\boldsymbol{v}}$ & $\bar{p}^d$	Zero stress	$\boldsymbol{n} \cdot (-\bar{p}^d \boldsymbol{I} + \bar{\nabla}\bar{\boldsymbol{v}} + (\bar{\nabla}\bar{\boldsymbol{v}})^T) = \boldsymbol{0}$
	$\bar{\psi}$	Dirichlet	$\bar{\psi} = 0$
	$\bar{\phi}$	Dirichlet	$\bar{\phi} = \bar{L}$
G-H-C-B	$\bar{\boldsymbol{v}}$ & $\bar{p}^d$	Zero stress	$\boldsymbol{n} \cdot (-\bar{p}^d \boldsymbol{I} + \bar{\nabla}\bar{\boldsymbol{v}} + (\bar{\nabla}\bar{\boldsymbol{v}})^T) = \boldsymbol{0}$
	$\bar{\psi}$	Dirichlet	$\bar{\psi} = 0$
	$\bar{\phi}$	Dirichlet	$\bar{\phi} = -\bar{L}$
B-C-D-A & C-H-E-D	$\bar{\boldsymbol{v}}$	Symmetry	$\boldsymbol{n} \cdot \bar{\boldsymbol{v}} = 0 \;\wedge\; \boldsymbol{n} \cdot \bar{\nabla}\bar{\boldsymbol{v}} = \boldsymbol{0}$
	$\bar{\psi}$	Symmetry	$\boldsymbol{n} \cdot \bar{\nabla}\bar{\psi} = 0$
	$\bar{\phi}$	Symmetry	$\boldsymbol{n} \cdot \bar{\nabla}\bar{\phi} = 0$
F-E-H-G & G-B-A-F	$\bar{\boldsymbol{v}}$ & $\bar{p}^d$	Zero stress	$\boldsymbol{n} \cdot (-\bar{p}^d \boldsymbol{I} + \bar{\nabla}\bar{\boldsymbol{v}} + (\bar{\nabla}\bar{\boldsymbol{v}})^T) = \boldsymbol{0}$
	$\bar{\psi}$	Dirichlet	$\bar{\psi} = 0$
	$\bar{\phi}$	Zero gradient	$\boldsymbol{n} \cdot \bar{\nabla}\bar{\phi} = 0$

our theory, we assume a spherical particle attached to a flat, undeformable interface, as shown in Fig. 6. We modeled the particle being attached to a cube having the side length of $(2L, L, L)$. According to Masliyah and Bhattacharjee [77], L has to be chosen such that $L \in [12a, 20a]$ to ensure that the results are virtually independent of the domain size. Nevertheless, the finiteness of the numerical domain limits the application for thick EDLs, whereas the spatial resolution of the mesh is a limiting factor for thin EDLs. We therefore limit the range of Debye parameters to $\kappa a \in [1, 10]$. We generate a fine and structured mesh in the EDL region, whereas an unstructured and much coarser mesh is employed everywhere else, since the highest gradients are expected in the proximity of the particle. In a simulation, we solve the set of Eqs. (2) and (4)–(6), together with the boundary conditions summarized in Table I. We used the predefined CFD and mathematics modules in COMSOL Multiphysics, for the hydrodynamic and the electrostatic equations, respectively. The Lagrangian shape functions used to discretize the variables are of second order, except of the first-order discretization of the pressure. The resulting system of algebraic equations is solved using the direct and fully coupled PARDISO solver. Henry's solution ($\Theta = 90°$) was used for validation, and errors smaller than 1% were obtained if we choose $L = 15a$. Consequently, we kept $L = 15a$ for all simulations. We calculate the electrophoretic mobility using Eq. (1) based on the mean value of the velocity at the plane A-D-E-F.

[1] A. Tiselius, A new apparatus for electrophoretic analysis of colloidal mixtures, Trans. Faraday Soc. **33**, 524 (1937).

[2] D. C. Schwartz and C. R. Cantor, Separation of yeast chromosome-sized DNAs by pulsed field gradient gel electrophoresis, Cell **37**, 67 (1984).

[3] O. Vesterberg, A short history of electrophoretic methods, Electrophoresis **14**, 1243 (1993).

[4] D. J. Harrison, A. Manz, Z. Fan, H. Luedi, and H. M. Widmer, Capillary electrophoresis and sample injection systems integrated on a planar glass chip, Anal. Chem. **64**, 1926 (1992).

[5] A. Manz, D. J. Harrison, E. M. J. Verpoorte, J. C. Fettinger, A. Paulus, H. Lüdi, and H. M. Widmer, Planar chips technology for miniaturization and integration of separation techniques into monitoring systems: capillary electrophoresis on a chip, J. Chromatogr. A **593**, 253 (1992).

[6] D. Mark, S. Haeberle, G. Roth, F. von Stetten, and R. Zengerle, Microfluidic lab-on-a-chip platforms: requirements, characteristics and applications, Chem. Soc. Rev. **39**, 1153 (2010).

[7] J. T. G. Overbeek, Theorie der Elektrophorese, Kolloid-Beihefte **54**, 287 (1943).

[8] R. W. O'Brien and L. R. White, Electrophoretic mobility of a spherical colloidal particle, J. Chem. Soc. Faraday Trans. 2 **74**, 1607 (1978).

[9] M. von Smoluchowski, Contribution to the theory of electro-osmosis and related phenomena, Bull. Int. Acad. Sci. Cracovie **3**, 184 (1903).

[10] E. Hückel, Die kataphorese der kugel, Physikalische Zeitschrift **25**, 204 (1924).

[11] D. C. Henry, The cataphoresis of suspended particles. Part I. The equation of cataphoresis, Proc. R. Soc. A **133**, 106 (1931).

[12] M. Fixman, Charged macromolecules in external fields. I. The sphere, J. Chem. Phys. **72**, 5177 (1980).

[13] F. A. Morrison, Electrophoresis of a particle of arbitrary shape, J. Colloid Interface Sci. **34**, 210 (1970).

[14] M. Teubner, The motion of charged colloidal particles in electric fields, J. Chem. Phys. **76**, 5564 (1982).

[15] F. Booth, The cataphoresis of spherical, solid nonconducting particles in a symmetrical electrolyte, Proc. R. Soc. A **203**, 514 (1950).

[16] P. H. Wiersema, A. L. Loeb, and J. T. G. Overbeek, Calculation of the electrophoretic mobility of a spherical colloid particle, J. Colloid Interface Sci. **22**, 78 (1966).

[17] H. J. Keh and J. L. Anderson, Boundary effects on electrophoretic motion of colloidal spheres, J. Fluid Mech. **153**, 417 (1985).

[18] H. J. Keh and T. H. Hsieh, Electrophoresis of a colloidal sphere in a spherical cavity with arbitrary zeta potential distributions and arbitrary double-layer thickness, Langmuir **24**, 390 (2008).

[19] Y.-W. Liu, S. Pennathur, and C. D. Meinhart, Electrophoretic mobility of a spherical nanoparticle in a nanochannel, Phys. Fluids **26**, 112002 (2014).

[20] Y.-W. Liu, S. Pennathur, and C. D. Meinhart, Electrophoretic mobility of spherical particles in bounded domain, J. Colloid Interface Sci. **461**, 32 (2016).

[21] L. D. Reed and F. A. Morrison, Hydrodynamic interactions in electrophoresis, J. Colloid Interface Sci. **54**, 117 (1976).

[22] A. A. Shugai, S. L. Carnie, D. Y. C. Chan, and J. L. Anderson, Electrophoretic motion of two spherical particles with thick double layers, J. Colloid Interface Sci. **191**, 357 (1997).

[23] E. Bormashenko, R. Pogreb, R. Balter, O. Gendelman, and D. Aurbach, Composite non-stick droplets and their actuation with electric field, Appl. Phys. Lett. **100**, 151601 (2012).

[24] T. Ngai and S. A. F. Bon, *Particle-stabilized Emulsions and Colloids* (Royal Society of Chemistry, London, 2014).

[25] N. S. Hush, The free energies of hydration of gaseous ions, Aust. J. Chem. **1**, 480 (1948).

[26] A. N. Frumkin, Note on B. Kamieński's paper, The nature of the electric potential at the free surface of aqueous solutions, Electrochim. Acta **2**, 351 (1960).

[27] K. Ciunel, M. Armélin, G. H. Findenegg, and R. von Klitzing, Evidence of surface charge at the air/water interface from thin-film studies on polyelectrolyte-coated substrates, Langmuir **21**, 4790 (2005).

[28] A. Bühl, Über die Potentialdifferenz in der Doppelschicht an der Oberfläche einfacher Elektrolyte und des reinen Wassers, Ann. Phys. **389**, 211 (1927).

[29] V. I. Parfenyuk, Surface potential at the gas-aqueous solution interface, Colloid J. **64**, 588 (2002).

[30] L. I. Krishtalik, The surface potential of solvent and the intraphase pre-existing potential, Russ. J. Electrochem. **44**, 43 (2008).

[31] F. H. Stillinger and A. Ben-Naim, Liquid-vapor interface potential for water, J. Chem. Phys. **47**, 4431 (1967).

[32] K. Leung, Surface potential at the air-water interface computed using density functional theory, J. Phys. Chem. Lett. **1**, 496 (2010).

[33] E. N. Brodskaya and V. V. Zakharov, Computer simulation study of the surface polarization of pure polar liquids, J. Chem. Phys. **102**, 4595 (1995).

[34] S. M. Kathmann, I.-F. W. Kuo, and C. J. Mundy, Electronic effects on the surface potential at the vapor-liquid interface of water, J. Am. Chem. Soc. **131**, 17522 (2009).

[35] M. Paluch, Surface potential at the water-air interface, Ann. Univ. Mariae Curie-Sklodowska, Sect. AA–Chemia **70**, 1 (2016).

[36] M. Chaplin, Theory versus experiment. What is the charge at the surface of water? Water J. **1**, 1 (2009).

[37] P. Tsai, J. Lou, Y.-Y. He, and E. Lee, Electrophoresis of a spherical particle normal to an air-water interface, Electrophoresis **31**, 3363 (2010).

[38] Y. Gao and D. Li, Translational motion of a spherical particle near a planar liquid-fluid interface, J. Colloid Interface Sci. **319**, 344 (2008).

[39] M. G. Nikolaides, A. R. Bausch, M. F. Hsu, A. D. Dinsmore, M. P. Brenner, and D. A. Weitz, Electric-field-induced capillary attraction between like-charged particles at liquid interfaces, Nature **420**, 299 (2002).

[40] R. Aveyard, B. P. Binks, J. H. Clint, P. D. I. Fletcher, T. S. Horozov, B. Neumann, V. N. Paunov, J. Annesley, S. W. Botchway, D. Nees, A. W. Parker, A. D. Ward, and A. N. Burgess, Measurement of Long-Range Repulsive Forces Between Charged Particles at an Oil-Water Interface, Phys. Rev. Lett. **88**, 246102 (2002).

[41] M. Megens and J. Aizenberg, Like-charged particles at liquid interfaces, Nature **424**, 1014 (2003).

[42] L. Foret and A. Würger, Electric-Field Induced Capillary Interaction of Charged Particles at a Polar Interface, Phys. Rev. Lett. **92**, 058302 (2004).

[43] K. D. Danov, P. A. Kralchevsky, and M. P. Boneva, Electrodipping force acting on solid particles at a fluid interface, Langmuir **20**, 6139 (2004).

[44] K. D. Danov and P. A. Kralchevsky, Electric forces induced by a charged colloid particle attached to the water-nonpolar fluid interface, J. Colloid Interface Sci. **298**, 213 (2006).

[45] K. D. Danov, P. A. Kralchevsky, and M. P. Boneva, Shape of the capillary meniscus around an electrically charged particle at a fluid interface: Comparison of theory and experiment, Langmuir **22**, 2653 (2006).

[46] K. D. Danov and P. A. Kralchevsky, Reply to comment on electrodipping force acting on solid particles at a fluid interface, Langmuir **22**, 848 (2006).

[47] M. Oettel, A. Domínguez, and S. Dietrich, Comment on electrodipping force acting on solid particles at a fluid interface, Langmuir **22**, 846 (2006).

[48] S. Kim and S. J. Karrila, *Microhydrodynamics: Principles and Selected Applications* (Courier Corporation, North Chelmsford, MA, 2013).

[49] A. Dörr and S. Hardt, Line tension and reduction of apparent contact angle associated with electric double layers, Phys. Fluids **26**, 082105 (2014).

[50] J. T. Petkov, N. D. Denkov, K. D. Danov, O. D. Velev, R. Aust, and F. Durst, Measurement of the drag coefficient of spherical particles attached to fluid interfaces, J. Colloid Interface Sci. **172**, 147 (1995).

[51] E. C. Mbamala and H. H. von Grünberg, Effective interaction of a charged colloidal particle with an air-water interface, J. Phys.: Condens. Matter **14**, 4881 (2002).

[52] B. J. Yoon and S. Kim, Electrophoresis of spheroidal particles, J. Colloid Interface Sci. **128**, 275 (1989).

[53] J. Y. Kim and B. J. Yoon, Electrophoretic motion of a slightly deformed sphere with a nonuniform zeta potential distribution, J. Colloid Interface Sci. **251**, 318 (2002).

[54] S. Barany, Electrophoresis in strong electric fields, Adv. Colloid Interface Sci. **147-148**, 36 (2009).

[55] J. R. Melcher, *Continuum Electromechanics*, Vol. 2 (MIT Press, Cambridge, MA, 1981).

[56] J. D. Jackson, *Classical Electrodynamics* (John Wiley & Sons, New York, 2007).

[57] L. G. Leal, *Advanced Transport Phenomena: Fluid Mechanics and Convective Transport Processes* (Cambridge University Press, Cambridge, 2007).

[58] A. Ramos, *Electrokinetics and Electrohydrodynamics in Microsystems* (Springer Science & Business Media, Berlin, 2011).

[59] Y. Wang and M. Oberlack, A thermodynamic model of multiphase flows with moving interfaces and contact line, Continuum Mech. Thermodyn. **23**, 409 (2011).

[60] A. Dörr and S. Hardt, Driven particles at fluid interfaces acting as capillary dipoles, J. Fluid Mech. **770**, 5 (2015).

[61] H. Brenner, The Stokes resistance of a slightly deformed sphere, Chem. Eng. Sci. **19**, 519 (1964).

[62] S. Senchenko and H. J. Keh, Thermophoresis of a slightly deformed aerosol sphere, Phys. Fluids **19**, 033102 (2007).

[63] A. S. Khair, Diffusiophoresis of colloidal particles in neutral solute gradients at finite Péclet number, J. Fluid Mech. **731**, 64 (2013).

[64] W. E. Byerly, *An Elementary Treatise on Fourier's Series: Spherical, Cylindrical, and Ellipsoidal Harmonics, with Applications to Problems in Mathematical Physics* (Dover Publications, London, 1893).

[65] T. M. MacRobert, *Spherical Harmonics: An Elementary Treatise on Harmonic Functions with Applications* (Methuen & Company Limited, London, 1947).

[66] D. Gilberg and N. S. Trudinger, *Elliptic Partial Differential Equations of Second Order* (Springer, Berlin, 2015).

[67] T. Chou, Geometry-Dependent Electrostatics Near Contact Lines, Phys. Rev. Lett. **87**, 106101 (2001).

[68] B. J. Kirby and E. F. Hasselbrink, Zeta potential of microfluidic substrates: 2. Data for polymers, Electrophoresis **25**, 203 (2004).

[69] *Comsol Multiphysics* (COMSOL®, Inc., Göttingen, Germany, 2017).

[70] G. Boniello, C. Blanc, D. Fedorenko, M. Medfai, N. B. Mbarek, M. In, M. Gross, A. Stocco, and M. Nobili, Brownian diffusion of a partially wetted colloid, Nat. Mater. **14**, 908 (2015).

[71] S.-N. Yin, C.-F. Wang, Z.-Y. Yu, J. Wang, S.-S. Liu, and S. Chen, Versatile bifunctional magnetic-fluorescent responsive Janus supraballs towards the flexible bead display, Adv. Mater. **23**, 2915 (2011).

[72] B. J. Park, T. Brugarolas, and D. Lee, Janus particles at an oil-water interface, Soft Matter **7**, 6413 (2011).

[73] H.-M. Gao, Z.-Y. Lu, H. Liu, Z.-Y. Sun, and L.-J. An, Orientation and surface activity of Janus particles at fluid-fluid interfaces, J. Chem. Phys. **141**, 134907 (2014).

[74] P. Dommersnes and J. O. Fossum, Surface structuring of particle laden drops using electric fields, Eur. Phys. J. Spec. Top. **225**, 715 (2016).

[75] G. Chen, P. Tan, S. Chen, J. Huang, W. Wen, and L. Xu, Coalescence of Pickering Emulsion Droplets Induced by an Electric Field, Phys. Rev. Lett. **110**, 064502 (2013).

[76] H. A. Lorentz, A general theorem concerning the motion of a viscous fluid and a few consequences derived from it, Zittingsverlag Akad. Wet. Amsterdam **5**, 168 (1896).

[77] J. H. Masliyah and S. Bhattacharjee, *Electrokinetic and Colloid Transport Phenomena* (John Wiley & Sons, New York, 2006).